1 **Phase-separated nuclear bodies of nucleoporin fusions, SET-NUP214 and NUP98-**
2 **HOXA9, promote condensation of MLL1 and CRM1 to activate target genes**
3

4 Masahiro Oka[1,2]*, Mayumi Otani[1], Yoichi Miyamoto[1], Jun Adachi[3], Takeshi Tomonaga[3],
5 Munehiro Asally[4], Yasuyuki Ohkawa[5]*, Yoshihiro Yoneda[6]
6

7 Author Affiliations
8 [1] Laboratory of Nuclear Transport Dynamics, National Institutes of Biomedical Innovation,
9   Health and Nutrition (NIBIOHN), Ibaraki, Osaka, Japan.
10 [2] Laboratory of Biomedical Innovation, Graduate School of Pharmaceutical Sciences, Osaka
11   University, Suita, Osaka, Japan.
12 [3] Laboratory of Proteome Research and Laboratory of Proteomics for Drug Discovery, National
13   Institutes of Biomedical Innovation, Health and Nutrition (NIBIOHN), Ibaraki, Osaka, Japan.
14 [4] School of Life Sciences, University of Warwick, United Kingdom.
15 [5] Department of Advanced Medical Initiatives, Faculty of Medicine, Kyushu University,
16   Fukuoka, Japan.
17 [6] National Institutes of Biomedical Innovation, Health and Nutrition (NIBIOHN), Ibaraki,
18   Osaka, Japan.
19

20 * Correspondence
21 Masahiro Oka, National Institutes of Biomedical Innovation, Health and Nutrition (NIBIOHN),
22 Ibaraki, Osaka, Japan; e-mail: moka@nibiohn.go.jp
23 Yasuyuki Ohkawa, Department of Advanced Medical Initiatives, Faculty of Medicine, Kyushu
24 University, Fukuoka, Japan; e-mail: yohkawa@kyushu.in
25
26

27 Key words: nucleoporin; NUP214; NUP98; MLL1; CRM1; leukemia; *HOX* cluster genes;
28 nuclear body; phase separation; molecular condensation; gene expression.
29

30 **ABSTRACT**
31

32 Nucleoporins NUP98 and NUP214 form chimeric fusion proteins that assemble into phase-
33 separated nuclear bodies. However, the function and physiological significance of these nuclear
34 bodies remain largely unknown. Previously, we reported that both NUP98-HOXA9 and SET-
35 NUP214 are recruited to *HOX* cluster regions via chromatin-bound CRM1, a nuclear export
36 receptor (Oka et al., 2019). Here, we show that these nuclear bodies promote the condensation
37 of mixed lineage leukemia 1 (MLL1), a histone methyltransferase which is essential for the
38 maintenance of *HOX* gene expression. Our analysis revealed that SET-NUP214 and CRM1
39 robustly associate with MLL1 to form nuclear bodies and are colocalized on chromatin. We also
40 showed that MLL1 and CRM1 are recruited to the nuclear bodies of NUP98-HOXA9 and that
41 the NUP98-HOXA9/CRM1/MLL1 complex accumulates on its target gene loci, including *HOX*

42   clusters and *MEIS1*. These phenomena were not observed in phase-separation–deficient mutants
43   or non-DNA-binding mutants of NUP98-HOXA9. Collectively, these results show that both
44   phase separation and proper targeting of nucleoporin fusions to specific sites could enhance the
45   activation of a wide range of target genes by promoting the condensation of MLL1 and CRM1.
46
47   **INTRODUCTION**
48
49   NUP98 and NUP214 are nucleoporins, the components of the nuclear pore complex
50   (NPC), and are often rearranged in leukemia (Lam and Aplan, 2001; Xu and Powers, 2009). The
51   nucleoporin fusion genes, produced by chromosomal translocation, are associated with
52   leukemogenesis: NUP98 fuses with various partner genes, including homeobox transcription
53   factors (Gough et al., 2011; Michmerhuizen et al., 2020); NUP214 fuses with its partner genes,
54   such as SET or DEK (Mendes and Fahrenkrog, 2019; Zhou and Yang, 2014).
55   Among NUP98 fusions, NUP98-HOXA9, a fusion between NUP98 and the homeobox
56   transcription factor HOXA9 (Borrow et al., 1996; Nakamura et al., 1996), is among the best
57   characterized fusion proteins to date. NUP98-HOXA9 causes aberrant gene expression that
58   contributes to leukemogenesis (Kroon et al., 2001).   Mechanistically, it is associated with
59   epigenetic modifiers, such as CREB-binding protein (CBP)/p300, HDAC1, and MLL1 (Bai et
60   al., 2006; Heikamp et al., 2021; Kasper et al., 1999; Mendes et al., 2020; Rio-Machin et al.,
61   2017; Shima et al., 2017; Xu et al., 2016). In addition, NUP98 itself is known to be associated
62   with trithorax (Trx), a Drosophila equivalent of MLL (Pascual-Garcia et al., 2014), or Wdr82–
63   Set1A/COMPASS, another H3K4 methyltransferase (Franks et al., 2017). SET-NUP214, a
64   fusion between NUP214 and the histone chaperone SET (von Lindern et al., 1992), also
65   interacts with MLL1 or DOT1L (Cigdem et al., 2021; Van Vlierberghe et al., 2008). These
66   studies suggest that the interaction between NUP fusion and these epigenetic modifiers likely
67   plays an important role in triggering aberrant gene expression.
68
69   Intriguingly, NUP98 and NUP214 fusion proteins share three characteristics: (i) both
70   contain dense FG repeats that are capable of forming nuclear bodies (Fornerod et al., 1995)
71   through phase separation (Labokha et al., 2013). (Notably, recent studies demonstrated that the
72   ability to form nuclear bodies of NUP98 fusion is important for aberrant gene activation and the
73   transformation of hematopoietic cells (Ahn et al., 2021; Chandra et al., 2021; Terlecki-
74   Zaniewicz et al., 2021)); (ii) their nuclear bodies colocalize with CRM1 (Oka et al., 2010; Oka
75   et al., 2016; Port et al., 2016; Saito et al., 2016; Saito et al., 2004; Takeda et al., 2010), a
76   nuclear export receptor (Fornerod et al., 1997; Fukuda et al., 1997; Ossareh-Nazari et al., 1997;
77   Stade et al., 1997) originally identified in fission yeast (Adachi and Yanagida, 1989); (iii) both
78   are associated with aberrant activation of *HOX* genes which encode the evolutionarily conserved
79   transcription factors that function in various developmental processes (Krumlauf, 1994). It is
80   known that *HOX* genes are dysregulated in various diseases and especially known to play a
81   crucial role in leukemogenesis (Alharbi et al., 2013; Argiropoulos and Humphries, 2007; Gough
82   et al., 2011; Grier et al., 2005; Hollink et al., 2011). Together, these studies suggest that the

83   formation of nuclear bodies containing CRM1 is a key feature of leukemogenic NUP fusions. In

84   support of this hypothesis, we recently found that CRM1 co-binds with NUP98- or NUP214-

85   fusion proteins to chromatin at specific gene loci, including *HOX* clusters (Oka et al., 2019; Oka

86   et al., 2016). In addition, CRM1 also facilitates the recruitment of SQSTM1-NUP214 (Gorello

87   et al., 2010) to *HOX* genes (Lavau et al., 2020).

88   Of note, chromatin-bound CRM1 may also play a role in other types of leukemia. It has

89   been shown that mutant NPM1 (NPM1c), the most frequent mutation in cytogenetically normal

90   acute myeloid leukemia generating a novel nuclear export signal (NES) at its C-terminus (Falini

91   et al., 2020; Falini et al., 2005; Schlenk et al., 2008), can activate *HOX* genes (Brunetti et al.,

92   2018), and also co-binds with CRM1 to the *HOX* cluster region (Oka et al., 2019). Moreover,

93   CALM-AF10, another NES-containing leukemogenic fusion protein, is also recruited to the

94   *HOX* cluster via CRM1 (Conway et al., 2015).

95   Despite this evidence, the molecular mechanism by which the formation of nuclear

96   bodies of NUP-fusion proteins linked to aberrant gene activation, especially its relationship with

97   epigenetic modifiers, remains largely unknown.

98   In this study, we investigated the potential role of NUP-fusion nuclear bodies in the

99   activation of its target genes. Our results suggested that the formation of NUP-fusion nuclear

100   bodies, which is dependent on CRM1, is important for promoting the condensation of MLL1 on

101   target sites to induce leukemogenic gene activation.

102

103   **RESULTS**

104

105   ***SET-NUP214 nuclear bodies colocalizes with HOX-B clusters***

106   SET-NUP214 forms CRM1-containing nuclear bodies in the human T-ALL cell line LOUCY

107   (Oka et al., 2019; Port et al., 2016). To evaluate the relevance of intranuclear localization of

108   nuclear bodies of SET-NUP214, we performed immunoFISH. We focused on *HOX-B* clusters

109   because our previous chromatin immunoprecipitation (ChIP)-seq data demonstrated that SET-

110   NUP214 and CRM1 robustly accumulated at several specific loci, especially *HOX-B* clusters in

111   LOUCY cells (Oka et al., 2019). Fluorescence microscopy images of *HOX-B* clusters and

112   immunostaining of SET-NUP214 nuclear bodies showed that they overlap in the nucleus

113   (Figure 1A, upper panel). To analyse this observation more quantitatively, we measured the

114   shortest distance between *HOX-B* and SET-NUP214 for each nuclear bodies (n=478). This

115   analysis revealed that 42.2 % of the nuclear bodies of SET-NUP214 were localized <0.2 μm

116   from *HOX-B* clusters (Figure 1B, blue). As a negative control, we also performed immunoFISH

117   for *RNF2* loci and the distance analysis (Figure 1A, lower, and Figure 1B, orange). Only 14.8 %

118   of SET-NUP214 nuclear bodies were found within <0.2 μm from *RNF2* loci. These results,

119   together with our previous ChIP-seq data, strongly suggest that the nuclear bodies of SET-

120   NUP214/CRM1 preferentially colocalize with the *HOX-B* cluster regions.

121

122   ***SET-NUP214/CRM1 physically and functionally associate with MLL1***

3

123   Next, we attempted to identify the constituents of SET-NUP214/CRM1 nuclear bodies

124   associated with chromatin. Taking advantage of the robust accumulation of SET-

125   NUP214/CRM1 on *HOX* clusters in LOUCY cells, we performed the rapid

126   immunoprecipitation mass spectrometry of endogenous proteins (RIME) (Figure 1C). This

127   method uses formaldehyde to crosslink protein complexes and DNA, similar to ChIP-

128   sequencing, and has been successfully used to identify chromatin-bound proteins associated

129   with target molecules (Mohammed et al., 2013). Our RIME data demonstrated that NUP214 and

130   CRM1 were strongly bound to each other, as their signals were primarily observed in both anti-

131   NUP214 and anti-CRM1 immunoprecipitates (IPs) (Table I). As expected, SET was found in

132   anti-NUP214 IPs, demonstrating that the SET-NUP214 fusion was successfully

133   immunoprecipitated. To find out the factors that are involved in the function of SET-

134   NUP214/CRM1 nuclear bodies, we focused on the proteins that are abundant both in anti-

135   NUP214 IPs and anti-CRM1 IPs, but not in control IPs (strict criteria were used to select the

136   candidate proteins whose peptide counts are either "0" or "1" in the control IP). We also found a

137   majority of nucleoporins (22 nucleoporins), together with nuclear transport receptors (NTRs) or

138   RAN and its regulators (Figure 1D, blue) in both IPs (Table I). We omitted these nucleoporins

139   or proteins involved in nuclear transport from our analysis since they are most likely the

140   association with endogenous NUP214 or CRM1 on NPCs. Interestingly, the analysis revealed

141   several proteins whose relationship with NPC or nuclear transport is not known to date, but are

142   strongly associated with both NUP214 and CRM1: namely, ADAR, MLL1, striatin, and

143   TRAF3IP(T3JAM) (Figure 1D). We also found MX2, an antiviral protein that interacts with

144   several nucleoporins (Dicks et al., 2018). We further analysed these five proteins.

145   Knockdowns of the five candidate genes were performed in LOUCY cells to monitor

146   the effect on the expression of *HOX* genes, which is dependent on SET-NUP214. The fold

147   change in *HOX* genes' expressions were measured in LOUCY cells by qPCR (Figure 1E). We

148   found that the knockdown of MLL1 substantially decreased the expression of *HOX* genes

149   (Figure 1E, Figure 1—figure supplement 1). We also found that knockdown of striatin, a

150   scaffold protein involved in the regulation of signaling pathways (Hwang and Pallas, 2014), also

151   decreased the expression of *HOX* genes. The knockdown of other candidate genes did not affect

152   *HOX* gene expression. Since the effect of MLL1 knockdown was more evident than that of

153   other knockdowns, we focused our analysis on MLL1.

154   To characterize MLL1, we costained the LOUCY cells with anti-MLL1 and anti-CRM1

155   antibodies (Figure 2, upper two columns). MLL1 frequently colocalized with SET-

156   NUP214/CRM1 nuclear bodies in LOUCY cells (Figure 2), which is consistent with recent

157   report (Cigdem et al., 2021). To examine if the partner proteins of MLL1 also colocalize with

158   the nuclear bodies, we immunostained Menin which has been shown to interact with MLL1

159   physically and functionally (Matkar et al., 2013; Yokoyama et al., 2005). The immunstaining

160   showed that Menin also colocalize with SET-NUP214/CRM1 nuclear bodies (Figure 2, third

161   column). In contrast, BRD4, a super-enhancer (SE)-enriched transcriptional coactivator that

162   often forms nuclear puncta (Sabari et al., 2018), only partially colocalized with SET-NUP214

163   nuclear bodies.

4

164

SET-NUP214/CRM1/MLL1 show genome-wide colocalization and are essential constituents
of the nuclear bodies

167   To further characterise the relevance of the association between MLL1, SET-NUP214,
168 and CRM1 in genome-wide binding, we performed ChIP-seq analysis (Figure 3A). Strikingly,
169 the binding sites of these proteins showed frequent co-occupancy on a genome-wide scale,
170 including *HOX-A* and *HOX-B* cluster regions (Figure 3A and 3B). Next, we examined the role
171 of MLL1 in SET-NUP214/CRM1 accumulation in *HOX* clusters. ChIP-qPCR analysis revealed
172 that MLL1 knockdown caused a significant decrease in SET-NUP214 signals in *HOX* clusters
173 (Figure 3C). Furthermore, CRM1 signals in the *HOX* clusters were significantly diminished.
174 These results suggested that binding of both SET-NUP214 and CRM1 to *HOX* cluster regions is
175 maintained by MLL1 and implicate that SET-NUP214, CRM1, and MLL1 form functional
176 nuclear bodies associated with *HOX* cluster regions to robustly activate *HOX* genes.

177   To investigate the role of CRM1 in this process, we used the CRM1 inhibitor KPT-330,
178 which covalently binds to CRM1 to inhibit its export activity and induces its degradation
179 (Etchin et al., 2013; Lapalombella et al., 2012; Mendonca et al., 2014; Tai et al., 2014; Turner et
180 al., 2013; Zhang et al., 2013) and disassembly of SET-NUP214 nuclear bodies (Oka et al.,
181 2019). First, immunostaining revealed that SET-NUP214 nuclear bodies colocalizing with
182 MLL1 diminished when incubated with 100 nM of KPT-330 for 24 h, and those were almost
183 completely disrupted at 1 µM (Figure 4A). Next, ChIP-seq and ChIP-qPCR were performed to
184 monitor the effect of KPT-330 treatment on the chromatin binding of MLL1 (Figure 3A, 4B).
185 The results showed that KPT-330 treatment caused a significant decrease in the signals of
186 MLL1 in *HOX* cluster regions, which is similar to the results observed in both CRM1 and SET-
187 NUP214. We also monitored the effect of KPT-330 on the MLL protein levels. As shown in
188 Figure 4C, our results showed that MLL1 protein levels were not significantly affected by KPT-
189 330. In addition, LMB, a CRM1 inhibitor that also disassembles nuclear bodies (Port et al.,
190 2016; Saito et al., 2016) and destabilizes the SET-NUP214 protein (Oka et al., 2019), without
191 inducing the degradation of CRM1, did not affect the levels of MLL1. Collectively, these results
192 suggest that CRM1 is critical for the assembly of SET-NUP214 nuclear bodies that can recruit
193 MLL1.

194

Phase separation and DNA binding of NUP98-HOXA9 are important for its targeting and
downstream gene activation

197   Previous reports suggested unexpected similarities between the nuclear bodies formed
198 by SET-NUP214 and NUP98-HOXA9; namely, they both accumulate on *HOX* cluster regions
199 (Oka et al., 2019; Oka et al., 2016; Van Vlierberghe et al., 2008; Xu et al., 2016) and contain
200 CRM1 (Oka et al., 2010; Oka et al., 2016; Saito et al., 2004; Takeda et al., 2010). NUP98-
201 HOXA9 is also known to be physically and functionally associated with MLL1 in
202 hematopoietic progenitor cells (Shima et al., 2017; Xu et al., 2016). However, the relevance of
203 the nuclear bodies of NUP98-HOXA9 to MLL1 remains unknown. These results prompted us to
204 investigate the relationship between MLL1 and the nuclear bodies formed by NUP98-HOXA9.

205   To investigate the function of NUP98-HOXA9, we isolated mouse ES cells (mESCs)
206 stably expressing FLAG-tagged NUP98-HOXA9 since we demonstrated that the *Hox* genes are
207 selectively activated in these cells (Oka et al., 2016). We first confirmed that our newly
208 established cell lines robustly activated *Hox* genes (Figure 5A). This analysis revealed that other
209 targets of NUP98-HOXA9 in transformed leukemia cells, *Meis1* and *Pbx3* (Takeda et al., 2006;
210 Xu et al., 2016), were also activated in these cells. This finding suggests that the mechanism of
211 NUP98-HOXA9-mediated gene activation is highly conserved between mESCs and
212 transformed leukemia cells.
213   To determine the importance of chromatin-associated nuclear bodies formed by
214 NUP98-HOXA9, we established cell lines carry mutated versions of NUP98-HOXA9. AG
215 mutant (mutated from FG to AG) is deficient in phase separation and N51S mutant (possessing
216 a point mutation in the homeodomain [N51S](Shanmugam et al., 1999)) is deficient to bind
217 DNA (Figure 5B). Introducing the AG mutation completely abolished the formation of nuclear
218 bodies, while N51S did not abolish the formation of nuclear bodies. However, these were fewer
219 and larger than that formed by wild-type NUP98-HOXA9 (Figure 5C), which is consistent with
220 previous studies (Ahn et al., 2021; Fahrenkrog et al., 2016).
221   These mutants enabled us to examine the importance of the formation of nuclear bodies
222 or their DNA-binding on accumulation in the *Hox* cluster region and gene activation.
223 Specifically, we compared ChIP data between NUP98-HOXA9 and its mutants. Our ChIP-seq
224 and qPCR results showed that the formation of nuclear bodies by FG repeats was important for
225 both the accumulation on *Hox* cluster genes and their robust activation (Figure 5A, D). In AG
226 mutant, the signals on *Hox* clusters were significantly diminished, and *Hox* gene activation was
227 completely lost. Thus, phase separation of NUP98-HOXA9 significantly contributes to its
228 targeting and concomitant gene activation. These results agree with a recent report using similar
229 mutant construct (FG to SG) expressed in hematopoietic stem and progenitor cells (Ahn et al.,
230 2021). Our results also showed that DNA-binding of nuclear bodies is important for the
231 targeting of NUP98-HOXA9, since the N51S mutation caused a drastic decrease in the ChIP-
232 signal on *Hox* clusters and terminated the activation of *Hox* genes.
233   Intriguingly, these phenomena were observed for target genes other than *Hox* clusters,
234 such as *Meis1* or *Pbx3*, in mESCs. Collectively, these results showed that the phase separation
235 and DNA-binding of NUP98-HOXA9 nuclear bodies, two distinct properties of the fusion that
236 rely on FG repeats and homeodomain, respectively, are important for targeting nuclear bodies
237 onto *Hox* clusters and other targets to activate downstream genes.
238
239 ***NUP98-HOXA9 nuclear bodies induce the condensation of CRM1 and MLL1 on its target***
240 ***loci***
241   Using these cell lines, we examined whether the nuclear bodies formed by NUP98-
242 HOXA9 are also related to MLL1. Strikingly, immunofluorescence analysis revealed that most
243 of the nuclear bodies formed by FLAG-NUP98-HOXA9 colocalized with MLL1 (Figure 6A).
244 We also noticed that these unusual staining patterns of MLL (obvious speckle formation) were
245 only observed in NUP98-HOXA9-expressing ES cells but not in parental ES cells, AG mutants,

246   or N51S homeodomain mutant expressing ES cells. Note that even if the robust NUP98-

247   HOXA9 nuclear bodies are formed in N51S mutant-expressing cells, MLL1 is not recruited in

248   these nuclear bodies. Therefore, our results suggested that both phase separation (via FG

249   repeats) and proper targeting to specific genome loci (via functional homeodomain) are

250   necessary for the formation of NUP98 nuclear bodies that could induce the sequestration of

251   MLL1. These results showed that nuclear bodies formed by NUP98-HOXA9 induce molecular

252   condensation of MLL1, which may increase the local concentration of MLL on *Hox* clusters or

253   other target loci.

254   To further investigate the role of NUP98-HOXA9 in the accumulation of MLL1 at the

255   target sites, we performed ChIP-seq analysis (Figure 6B–D, Figure 6—figure supplement 1).

256   We found that MLL1 (both MLL1N and MLL1C) weakly bound to the *Hox* cluster and other

257   target regions in parental ES cells. However, MLL1 robustly accumulated on the target sites in

258   the cell line expressing FLAG-NUP98-HOXA9. As for CRM1, we previously demonstrated that

259   ChIP-seq peaks of CRM1 were significantly enhanced in FLAG-NUP98-HOXA9 expressing

260   cells as compared with parental ES cells, using polyclonal anti-CRM1 antibody (Oka et al.,

261   2016). Here, we noticed that ChIP-seq using monoclonal anti-CRM1 antibody (CST) showed

262   marked differences in CRM1 ChIP signals between parental ES cells and FLAG-NUP98-

263   HOXA9 expressing cells (Figure 6B–D).

264   We further performed ChIP-qPCR and found that these effects were only observed in

265   the *Hox* cluster region in wild-type NUP98-HOXA9-expressing cells but not in AG or N51S

266   mutants (Figure 7A). In addition, correlation plot showed that there were strong positive

267   correlations between the binding sites of CRM1 and MLL1 in parental ES cells, and those were

268   significantly enhanced by the expression of FLAG-NUP98-HOXA9 (Figure 7B).

269   Together, these results showed that NUP fusion is capable of forming molecular

270   condensates with CRM1 and MLL1, which induce and/or maintain the activation of a wide

271   range of its targets.

272

273   **DISCUSSION**

274

275   In this study, we demonstrated that two NUP fusions, SET-NUP214 and NUP98-

276   HOXA9, drive the formation of nuclear bodies containing CRM1 and MLL1. Especially, our

277   results showed that phase separation of NUP fusions induces the condensation of MLL1 on

278   specific target sites.

279   MLL1 has been implicated in NUP fusion activity. NUP98-HOXA9 has been shown to

280   be associated with MLL1 and is required for its recruitment to target sites, including *HOX*

281   clusters, and downstream gene activation (Shima et al., 2017; Xu et al., 2016). Moreover, MLL1

282   knockout prevents NUP98-HOXA9-driven leukemogenesis (Shima et al., 2017; Xu et al.,

283   2016). In addition, SET-NUP214 has also been demonstrated to be associated with MLL1 and

284   to cooperatively enhance the transcription of *HOXA10* (Cigdem et al., 2021).

285   Here, our results suggested that NUP fusions and MLL1 not only interact with each

286   other but they are both essential constituents of molecular condensate (i.e., nuclear bodies) that

7

287   are presumably suitable for the simultaneous activation of several *HOX* genes that span tens of
288   kb apart, as observed in leukemia cells. MLL1, a histone methyltransferase, and its associated
289   molecules are most likely primary molecules for the creation of this molecular environment for
290   gene activation. However, we cannot exclude the possibility that other unknown factors could
291   also be recruited to achieve robust gene activation through phase separation. Our study further
292   demonstrated that these NUP bodies are maintained in a CRM1-dependent manner.

293   How these NUP bodies function and why their NUP properties are important? In
294   addition, the reason why only NUP98 and NUP214, among 30 different nucleoporins, are
295   frequently found in leukemogenic fusion remains unknown. A common characteristic of NUP98
296   FG and NUP214 FG is the existence of dense FG repeat sequences. These FGs can form FG
297   hydrogels *in vitro* (Labokha et al., 2013). In particular, Nup98 FG domains, which contain
298   GLFG motifs, are highly cohesive. NUP98, even from various species, can be shown to phase
299   separate to create FG particles (Schmidt and Gorlich, 2015). All these NUP bodies show unique
300   features, namely they repel inert macromolecules, yet allow the entrance of NTRs associated
301   with their cargoes.

302   Because CRM1 can penetrate the FG hydrogel with its cargo (Labokha et al., 2013), we
303   speculate that NUP98FG or NUP214FG could efficiently hold CRM1 and its associated
304   molecules (including MLL1) into the same condensates through phase separation. However, the
305   way that CRM1 associates with MLL1 and whether MLL1 contains a functional NES remains
306   unclear.

307   MLL encodes a large protein that is proteolytically cleaved into two fragments, MLL-N
308   and MLL-C (Hsieh et al., 2003; Yokoyama et al., 2002). Interestingly, MLL1 is known to form
309   nuclear speckles (Yano et al., 1997) in which both MLL-N and MLL-C fragments colocalize
310   (Hsieh et al., 2003). In addition, the prediction of disordered residues using IUPred2A
311   (Meszaros et al., 2018) suggested the presence of significant intrinsically disordered regions
312   (IDRs) in full-length MLL1(Figure 7—figure supplement 1). This suggests that MLL1 is prone
313   to phase separation, and its interaction with NUP fusions or CRM1 may further stimulate the
314   formation of nuclear bodies on chromatin. In fact, the binding profiles revealed by ChIP-seq
315   showed that NUP fusion, together with MLL1 and CRM1, binds to an unusually wide span of
316   target gene loci. Thus, the formation of NUP-fusion nuclear bodies on chromatin seems suitable
317   for creating a molecular environment for the simultaneous activation of multiple target genes
318   located in the neighborhood, as represented by the *HOX-A* cluster genes.

319   In a recent study, Ahn et al. showed that FG-mediated LLPS (Liquid-Liquid Phase
320   Separation) of NUP98-HOXA9 is important for the induction of an aberrant three-dimensional
321   chromatin structure that promotes malignant transformation (Ahn et al., 2021). They observed
322   that DNA loops were specifically formed in NUP98-HOXA9 overexpressed 293FT cells.
323   Furthermore, they found that the loops frequently overlapped with H3K27Ac marks. However,
324   an interactome study using BioID suggested that both wild-type and phase-separation-deficient
325   NUP98-HOXA9 (FG to SG mutant) shared most of their interacting proteins, including MLL1.
326   In contrast, our results demonstrated that NUP98-HOXA9, but not its phase-separation-deficient
327   mutant nor DNA-binding deficient mutant, could induce the condensation of MLL1 around its

328   target sites, including the *HOX-A* cluster region (Figure 7C). Collectively, the nuclear bodies

329   formed by NUP98-HOXA9 may be important for both three-dimensional chromatin architecture

330   as well as recruitment and/or concentration of MLL1. Future studies are needed to elucidate the

331   relationship between molecular condensation, higher-order chromatin stricture, and gene

332   activation, which are all triggered by the nuclear bodies of NUP fusions.

333

334   **MATERIALS AND METHODS**

335

336   *Cell culture*

337   The leukemia cell line LOUCY was cultured in RPMI1640 medium (Sigma) supplemented with

338   20% fetal bovine serum (FBS) (Sigma). EB3 ES cells (Niwa et al., 2002; Ogawa et al., 2004),

339   NUP98-HOXA9 stable ES cell lines or their derivatives were cultured as described previously

340   (Oka et al., 2016).

341

342   *RIME*

343   RIME was performed as previously described (Mohammed et al., 2016). Briefly, 1.5×10^7

344   LOUCY cells per condition were collected and fixed in serum-free RPMI medium

345   supplemented with 1% (v/v) formaldehyde for 8 min at room temperature. After the addition of

346   a final 0.1 M glycine to quench crosslinking, cells were washed twice with ice-cold phosphate-

347   buffered saline (PBS) and resuspended in 500 μL of PBS. After removal of the supernatants, the

348   cell pellets were snap-frozen in liquid N_2 and stored at -80 °C. The nuclear fraction of the cells

349   was extracted by resuspending the pellet in 10 mL of LB1 buffer (50 mM HEPES-KOH [pH

350   7.5], 140 mM NaCl, 1 mM EDTA, 10% glycerol, 0.5% Igepal CA-630, and 0.25% Triton X-

351   100) for 10 min at 4 °C with rotation. The cells were collected and resuspended in 10 mL of

352   LB2 buffer (10 mM Tris-HCl [pH 8.0], 200 mM NaCl, 1 mM EDTA, and 0.5 mM EGTA) and

353   incubated at 4 °C for 5 min with rotation. Cells were pelleted and resuspended in 300 mL of

354   LB3 buffer (10 mM Tris-HCl [pH 8], 100 mM NaCl, 1 mM EDTA, 0.5 mM EGTA, 0.1% Na-

355   deoxycholate, and 0.5% N-lauroylsarcosine) and sonicated in a water bath sonicator (Diagenode

356   Bioruptor; on ice, 30 s on/off cycle for 20 min). After the addition of 30 μL 10% (v/v) Triton X-

357   100, the samples were vortexed and centrifuged at 20,000 x g for 10 min to remove cell debris.

358   The supernatant was then added to 100 μL of magnetic beads (Dynal), preincubated with

359   antibody, and immunoprecipitation (IP) was performed at 4 °C overnight. The beads were then

360   washed with 1 mL of RIPA buffer 10 times and sequentially washed with freshly prepared 100

361   mM ammonium hydrogen carbonate (AMBIC) solution. For the second AMBIC wash, beads

362   were transferred to new tubes. After removing the supernatant, the samples were stored at –

363   80 °C.

364   To prepare the magnetic beads bound to the antibody, 100 μL of magnetic beads

365   (Dynal) was resuspended in 1 mL of PBS w/5 mg/mL BSA (PBS/BSA) and washed four times

366   with a magnetic separator. After resuspension in 500 μL of PBS/BSA, each antibody was added

367 and incubated overnight with rotation. The next day, the beads were washed five times with
368 PBS/BSA and used for IP.
369   Bead-bound protein was digested with 100 ng trypsin (Promega, V5113) overnight at
370 37 °C. After the overnight digest, 100 ng of trypsin was added to each sample and digested for 4
371 h at 37 °C. The digested peptides were acidified with TFA, desalted, and purified on C18-SCX
372 StageTips (Adachi et al., 2016). The peptides were dried with SpeedVac and solubilized with
373 0.1% formic acid/2% acetonitrile.
374
375 ***Liquid chromatography with tandem mass spectrometry (LC-MS/MS) analysis***
376 LC-MS/MS was performed by coupling an UltiMate 3000 Nano LC system (Thermo Fisher
377 Scientific) and HTC-PAL autosampler (CTC Analytics) to a Q Exactive hybrid quadrupole-
378 Orbitrap mass spectrometer (Thermo Fisher Scientific). The peptides were delivered to an
379 analytical column (75 μm × 30 cm, packed in-house with ReproSil-Pur C18-AQ, 1.9 μm resin,
380 Dr. Maisch, Ammerbuch, Germany) and separated at a flow rate of 280 nL/min using a 145 min
381 gradient from 5% to 30% of solvent B (solvent A, 0.1% FA and 2% acetonitrile; solvent B,
382 0.1% FA, and 90% acetonitrile). The Q Exactive instrument was operated in data-dependent
383 mode. Survey full-scan MS spectra (*m/z* 350–1,800) were acquired in the Orbitrap with 70,000
384 resolution after the accumulation of ions to a 3×10^6 target value. Dynamic exclusion was set at
385 30 s. The 12 most intense multiplied charged ions ($z \geq 2$) were sequentially accumulated to a 1
386 $\times 10^5$ target value and fragmented in the collision cell by higher energy collisional dissociation
387 (HCD) with a maximum injection time of 120 ms and 35,000 resolution. Typical mass
388 spectrometric conditions were as follows: spray voltage, 2 kV; heated capillary temperature,
389 250 °C; normalized HCD collision energy, 25%. The MS/MS ion selection threshold was set to
390 2.5×10^4 counts. A 2.0 Da isolation width was chosen.
391
392 ***Data processing and visualization***
393 Raw MS data were processed using MaxQuant (version 1.6.14.0), supported by the Andromeda
394 search engine. The MS/MS spectra were searched against the UniProt human database with the
395 following search parameters: full tryptic specificity; up to two missed cleavage sites;
396 carbamidomethylation of cysteine residues set as a fixed modification; serine, threonine, and
397 tyrosine phosphorylation, N-terminal protein acetylation; and methionine oxidation as variable
398 modifications. The false discovery rate of the protein groups and peptides was less than 0.01.
399 Peptides identified from the reversed database or those identified as potential contaminants were
400 not used.
401
402 ***ImmunoFISH***
403 ImmunoFISH was performed as previously described (Chaumeil et al., 2013). LOUCY cells
404 were pelleted, resuspended in a small volume of PBS, and placed on a poly L-lysine-coated
405 coverslip (Neuvitro Corporation, H-15-PDL). After the fixation of cells in 2%
406 paraformaldehyde/1x PBS for 10 min at room temperature, cells were washed three times in
407 PBS and permeabilized with ice-cold 0.4% Triton-X-100 in PBS for 5 min on ice. Then, the

10

408   cells were incubated in 100 µL of blocking solution for 30 min at room temperature and
409   incubated with the primary antibody in 100 µL of blocking solution for 1 h at room temperature.
410   After washing the cells in 0.2% BSA/0.1% Tween-20/PBS three times for 5 min each, the cells
411   were incubated with the secondary antibody diluted in 100 µL of blocking solution for 1 h. The
412   cells were washed three times with 0.1% Tween-20/PBS for 5 min each and fixed in 2%
413   paraformaldehyde/PBS for 10 min. After three washes with PBS, cells were incubated with 0.1
414   µg/µL RNase A (Nippon Gene) in PBS for 1 h at 37 °C in FISH slide processing system
415   (Thermobrite, ABBOTT). Cells were washed with PBS three times and permeabilized in ice-
416   cold 0.7% Triton-X-100/0.1 M HCl for 10 min on ice. After three washes with PBS, the cells
417   were incubated in 50% formamide/2x SSC at 75 °C for 30 min and hybridized with pre-labelled
418   BAC probes (RPCI-11 29G13 labelled red for *HOX-B*(chr17) and RPCI-11 44L12 labelled
419   green for *RNF2*(chr1); Empire Genomics) overnight at 37 °C using FISH slide processing
420   system. The next day, the cells were washed three times in 50% formamide/2x SSC, 5 min each
421   at 37 °C, followed by another three washes in 2x SSC (the last wash was performed with 2x
422   SSC containing 4',6-diamidino-2-phenylindole (DAPI), 5 min each at 37 °C. Cells were
423   mounted in ProLong Gold mounting medium (Thermo Fisher Scientific), and observed using a
424   SP8 confocal microscope (Leica). To evaluate the distance between SET-NUP214 and each
425   genomic locus, z-stack confocal images of SET-NUP214 and FISH were projected in 2D using
426   max z projection function in imageJ. Projecected images were binarized and NUP214 particles
427   were registed by imageJ roi manager. The distance from gene loci were then calculated using
428   distance map function of imageJ. The closest distance from gene loci were then calculated by
429   measuring the minimum intensity in the distance map.
430

431   ***Plasmids, isolation of stable ES cell lines***
432   Stable ES cell lines were generated as previously described (Oka et al., 2016). Briefly, parental
433   ES cells were transfected with pCAGGS-m2TP, an expression vector for Tol2 transposase, and
434   pT2A-CMH-FLAG-NUP98-HOXA9 or its mutants (Kawakami and Noda, 2004; Urasaki et al.,
435   2006) using Lipofectamine 2000 (Life Technologies). After 2 days, the cells were trypsinized
436   and replated onto ES-LIF medium containing hygromycin B (200 µg/mL). Colonies were
437   picked, and the expression of FLAG-NUP98-HOXA9 or its mutants was examined by
438   immunoblotting and immunofluorescence staining. cDNA encoding NUP98-HOXA9 has been
439   previously described (Oka et al., 2016), whereas DNA encoding the AG mutant of NUP98-
440   HOXA9 was synthesized (GenScript)(supplememntal file 1), or the homeodomain (N51S)
441   mutant of NUP98-HOXA9 was generated by PCR-based mutagenesis, and cloned into pT2A-
442   CMH-FLAGx3.
443

444   ***Immunostaining and confocal microscopy***
445   Human leukemia LOUCY cells were attached onto poly L-lysine-coated coverslips (Neuvitro
446   Corporation, H-15-PDL) and fixed in PBS containing 3.7% formaldehyde for 15 min at room
447   temperature. The cells were washed with PBS and permeabilized with 0.5% Triton X-100 in
448   PBS for 5 min at room temperature. After washing with PBS, the cells were incubated with

11

449 blocking buffer (3% skim milk in PBS) for 30 min. The cells were incubated with primary
450 antibodies overnight, washed three times with PBS, and incubated with secondary antibodies for
451 30 min. The cells were washed twice with PBS and stained with DAPI in PBS for 15 min at
452 room temperature. The cells were mounted using ProLong Gold (Thermo Fisher Scientific).
453 Images were acquired using a SP8 confocal microscope (Leica). ES cells were grown on
454 coverslips and fixed in a medium containing 3.7% formaldehyde for 15 min at room
455 temperature. After washing with PBS, the cells were permeabilized with 0.5% Triton X-100 in
456 PBS for 5 min and further incubated with a blocking buffer (3% skim milk in PBS) for 30 min.
457 Next, cells were incubated with primary antibodies overnight at 4 °C. After washing four times
458 with PBS, the cells were incubated with secondary antibodies for 30 min. Cells were washed
459 four times with PBS, stained with DAPI for 15 min at room temperature, and the coverslips
460 were mounted with ProLong Gold mounting medium (Thermo Fischer Scientific). Images were
461 acquired using a SP8 confocal microscope (Leica).
462

463 ***ChIP-qPCR, ChIP-seq***
464 ChIP-qPCR and ChIP-seq were performed as previously described (Oka et al., 2019). Human
465 leukemia LOUCY cells were fixed in a medium containing 0.5% formaldehyde at room
466 temperature for 5 min. Fixed cells were collected by centrifugation at room temperature, washed
467 twice with ice-cold PBS, and resuspended in ChIP buffer (10 mM Tris-HCl pH 8.0, 200 mM
468 KC), 1 mM CaCl2, 0.5% NP40) containing protease inhibitors (2 μg/mL aprotinin, 2 μg/mL
469 leupeptin, and 1 μg/mL pepstatin A). Cells were briefly sonicated (Branson 250D Sonifier,
470 Branson Ultrasonics), and after centrifugation, the supernatants were digested with 1 U/mL
471 micrococcal nuclease (Worthington Biochemical) for 40 min at 37 °C. The reaction was stopped
472 with EDTA (final concentration of 10 mM), and the supernatants were incubated with anti-
473 mouse or anti-rabbit IgG magnetic beads (Dynabeads, Life Technologies) preincubated with
474 anti-FLAG M2 (Sigma), anti-CRM1 (CST or Bethyl Lab), anti-NUP214 (Bethyl Lab), anti-
475 MLL1C (CST), and anti-MLL1N (CST) for 6 h. The beads were washed twice with each of the
476 following buffers: ChIP buffer, ChIP wash buffer (10 mM Tris-HCl pH 8.0, 500 mM KCl, 1
477 mM CaCl2, 0.5% NP40), and TE buffer (10 mM Tris-HCl pH 8.0, 1 mM EDTA) and eluted in
478 an elution buffer containing 50 mM Tris-HCl pH 8.0, 10 mM EDTA, and 1% sodium dodecyl
479 sulfate overnight at 65 °C. DNA was recovered using AMPure XP beads (Beckman Coulter)
480 and used for ChIP-qPCR analysis or for library preparation for ChIP-seq analysis.
481 For ES cells, cells grown in dishes were fixed in medium containing 0.5% formaldehyde at
482 room temperature for 5 min. After one wash with ice-cold PBS, PBS (0.5 mL) was added, and
483 cells were collected with a scraper. After centrifugation, the collected fixed cells were processed
484 as described above for LOUCY cells.
485 The ChIP library was prepared using ThruPLEX DNA-seq kit (Takara Bio), according
486 to the manufacturer's instructions, and sequenced on the Illumina HiSeq1500 or NovaSeq 6000
487 system. Adaptor sequence and low quality sequence were removed and read length below 20bp
488 were discarded by using Trim Galore (version 0.6.70). The sequence reads were aligned to the
489 reference mouse genome (mm10) and human genome (GRCh38) using Bowtie2 (version 2.3.1).

12

490   Multi-mapping and duplicated reads were not used for further analysis. ChIP peaks were
491   indentified by using MACS2 (version 2.2.7.1) with p-value < 0.001.
492
493   *qPCR*
494   Total RNA was extracted from cells using the MagMAX mirVana Total RNA kit (Thermo
495   Fisher Scientific) using King Fischer Duo (Thermo Fisher Scientific) or ReliaPrep RNA
496   Miniprep Systems (Promega) and used for cDNA synthesis with the PrimeScript RT reagent Kit
497   (Takara Bio). All procedures were performed in accordance with the manufacturer's protocol.
498   qPCR analysis was performed on a 384-well plate with the QuantStudio 6 Flex Real-Time PCR
499   System (Life Technologies) using GeneAce SYBR qPCR Mix (Nippon Gene). The relative
500   gene expression levels were normalized to *GAPDH* mRNA levels as a control. The primer
501   sequences are listed in Supplementary File 1.
502
503   *Gene knockdown*
504   Gen knockdown in LOUCY cells was performed as previously described (Oka et al., 2019).
505   Briefly, LOUCY cells (1×10^7 cells) were transfected with 4 µM of each siRNA (TriFECTa®
506   RNAi Kit, IDT) or negative control siRNA (Universal Negative Control siRNA [Nippon Gene])
507   by nucleofection (Lonza) using reagent V and the X-001 program. Immediately after
508   nucleofection, the cells were plated on a 100 mm dish in RPMI 1640 medium supplemented
509   with 20% FBS for the indicated period and used for immunoblotting and ChIP-qPCR.
510
511   *Accession numbers*
512   The ChIP-Seq data are accessible through GEO Series accession number GSE202837.
513
514   *Statistical analysis*
515   Statistical analyses were performed using an unpaired two-tailed Student's *t*-test. GraphPad
516   Prism version 8 was used for data analysis and representation.
517

527
528

REFERENCES

Adachi, J., Hashiguchi, K., Nagano, M., Sato, M., Sato, A., Fukamizu, K., Ishihama, Y., and Tomonaga, T. (2016). Improved Proteome and Phosphoproteome Analysis on a Cation Exchanger by a Combined Acid and Salt Gradient. Anal Chem *88*, 7899-7903.

Adachi, Y., and Yanagida, M. (1989). Higher order chromosome structure is affected by cold-sensitive mutations in a Schizosaccharomyces pombe gene crm1+ which encodes a 115-kD protein preferentially localized in the nucleus and its periphery. The Journal of cell biology *108*, 1195-1207.

Ahn, J.H., Davis, E.S., Daugird, T.A., Zhao, S., Quiroga, I.Y., Uryu, H., Li, J., Storey, A.J., Tsai, Y.H., Keeley, D.P.*, et al.* (2021). Phase separation drives aberrant chromatin looping and cancer development. Nature *595*, 591-595.

Alharbi, R.A., Pettengell, R., Pandha, H.S., and Morgan, R. (2013). The role of HOX genes in normal hematopoiesis and acute leukemia. Leukemia *27*, 1000-1008.

Argiropoulos, B., and Humphries, R.K. (2007). Hox genes in hematopoiesis and leukemogenesis. Oncogene *26*, 6766-6776.

Bai, X.T., Gu, B.W., Yin, T., Niu, C., Xi, X.D., Zhang, J., Chen, Z., and Chen, S.J. (2006). Trans-repressive effect of NUP98-PMX1 on PMX1-regulated c-FOS gene through recruitment of histone deacetylase 1 by FG repeats. Cancer research *66*, 4584-4590.

Borrow, J., Shearman, A.M., Stanton, V.P., Jr., Becher, R., Collins, T., Williams, A.J., Dube, I., Katz, F., Kwong, Y.L., Morris, C.*, et al.* (1996). The t(7;11)(p15;p15) translocation in acute myeloid leukaemia fuses the genes for nucleoporin NUP98 and class I homeoprotein HOXA9. Nature genetics *12*, 159-167.

Brunetti, L., Gundry, M.C., Sorcini, D., Guzman, A.G., Huang, Y.H., Ramabadran, R., Gionfriddo, I., Mezzasoma, F., Milano, F., Nabet, B.*, et al.* (2018). Mutant NPM1 Maintains the Leukemic State through HOX Expression. Cancer cell *34*, 499-512 e499.

Chandra, B., Michmerhuizen, N.L., Shirnekhi, H.K., Tripathi, S., Pioso, B.J., Baggett, D.W., Mitrea, D.M., Iacobucci, I., White, M.R., Chen, J.*, et al.* (2021). Phase Separation mediates NUP98 Fusion Oncoprotein Leukemic Transformation. Cancer discovery.

Chaumeil, J., Micsinai, M., and Skok, J.A. (2013). Combined immunofluorescence and DNA FISH on 3D-preserved interphase nuclei to study changes in 3D nuclear organization. J Vis Exp, e50087.

Cigdem, S., Saito, S., Nishikata, D., Nagata, K., and Okuwaki, M. (2021). SET-NUP214 and MLL cooperatively regulate the promoter activity of the HoxA10 gene. Genes to cells : devoted to molecular & cellular mechanisms *26*, 830-837.

Conway, A.E., Haldeman, J.M., Wechsler, D.S., and Lavau, C.P. (2015). A critical role for CRM1 in regulating HOXA gene transcription in CALM-AF10 leukemias. Leukemia *29*, 423-432.

Dicks, M.D.J., Betancor, G., Jimenez-Guardeno, J.M., Pessel-Vivares, L., Apolonia, L., Goujon, C., and Malim, M.H. (2018). Multiple components of the nuclear pore complex interact with the amino-terminus of MX2 to facilitate HIV-1 restriction. PLoS Pathog *14*, e1007408.

14

570 Etchin, J., Sun, Q., Kentsis, A., Farmer, A., Zhang, Z.C., Sanda, T., Mansour, M.R., Barcelo, C.,
571   McCauley, D., Kauffman, M., *et al.* (2013). Antileukemic activity of nuclear export
572   inhibitors that spare normal hematopoietic cells. Leukemia *27*, 66-74.
573 Fahrenkrog, B., Martinelli, V., Nilles, N., Fruhmann, G., Chatel, G., Juge, S., Sauder, U., Di
574   Giacomo, D., Mecucci, C., and Schwaller, J. (2016). Expression of Leukemia-Associated
575   Nup98 Fusion Proteins Generates an Aberrant Nuclear Envelope Phenotype. PloS one *11*,
576   e0152321.
577 Falini, B., Brunetti, L., Sportoletti, P., and Martelli, M.P. (2020). NPM1-mutated acute myeloid
578   leukemia: from bench to bedside. Blood *136*, 1707-1721.
579 Falini, B., Mecucci, C., Tiacci, E., Alcalay, M., Rosati, R., Pasqualucci, L., La Starza, R.,
580   Diverio, D., Colombo, E., Santucci, A., *et al.* (2005). Cytoplasmic nucleophosmin in acute
581   myelogenous leukemia with a normal karyotype. N Engl J Med *352*, 254-266.
582 Fornerod, M., Boer, J., van Baal, S., Jaegle, M., von Lindern, M., Murti, K.G., Davis, D.,
583   Bonten, J., Buijs, A., and Grosveld, G. (1995). Relocation of the carboxyterminal part of
584   CAN from the nuclear envelope to the nucleus as a result of leukemia-specific chromosome
585   rearrangements. Oncogene *10*, 1739-1748.
586 Fornerod, M., Ohno, M., Yoshida, M., and Mattaj, I.W. (1997). CRM1 is an export receptor for
587   leucine-rich nuclear export signals. Cell *90*, 1051-1060.
588 Franks, T.M., McCloskey, A., Shokirev, M.N., Benner, C., Rathore, A., and Hetzer, M.W.
589   (2017). Nup98 recruits the Wdr82-Set1A/COMPASS complex to promoters to regulate
590   H3K4 trimethylation in hematopoietic progenitor cells. Genes Dev *31*, 2222-2234.
591 Fukuda, M., Asano, S., Nakamura, T., Adachi, M., Yoshida, M., Yanagida, M., and Nishida, E.
592   (1997). CRM1 is responsible for intracellular transport mediated by the nuclear export
593   signal. Nature *390*, 308-311.
594 Gorello, P., La Starza, R., Di Giacomo, D., Messina, M., Puzzolo, M.C., Crescenzi, B., Santoro,
595   A., Chiaretti, S., and Mecucci, C. (2010). SQSTM1-NUP214: a new gene fusion in adult T-
596   cell acute lymphoblastic leukemia. Haematologica *95*, 2161-2163.
597 Gough, S.M., Slape, C.I., and Aplan, P.D. (2011). NUP98 gene fusions and hematopoietic
598   malignancies: common themes and new biologic insights. Blood *118*, 6247-6257.
599 Grier, D.G., Thompson, A., Kwasniewska, A., McGonigle, G.J., Halliday, H.L., and Lappin,
600   T.R. (2005). The pathophysiology of HOX genes and their role in cancer. J Pathol *205*, 154-
601   171.
602 Heikamp, E.B., Henrich, J.A., Perner, F., Wong, E.M., Hatton, C., Wen, Y., Barwe, S.P.,
603   Gopalakrishnapillai, A., Xu, H., Uckelmann, H.J., *et al.* (2021). The Menin-MLL1
604   interaction is a molecular dependency in NUP98-rearranged AML. Blood.
605 Hollink, I.H., van den Heuvel-Eibrink, M.M., Arentsen-Peters, S.T., Pratcorona, M., Abbas, S.,
606   Kuipers, J.E., van Galen, J.F., Beverloo, H.B., Sonneveld, E., Kaspers, G.J., *et al.* (2011).
607   NUP98/NSD1 characterizes a novel poor prognostic group in acute myeloid leukemia with a
608   distinct HOX gene expression pattern. Blood *118*, 3645-3656.

609   Hsieh, J.J., Ernst, P., Erdjument-Bromage, H., Tempst, P., and Korsmeyer, S.J. (2003).
610   Proteolytic cleavage of MLL generates a complex of N- and C-terminal fragments that
611   confers protein stability and subnuclear localization. Mol Cell Biol *23*, 186-194.
612   Hwang, J., and Pallas, D.C. (2014). STRIPAK complexes: structure, biological function, and
613   involvement in human diseases. Int J Biochem Cell Biol *47*, 118-148.
614   Kasper, L.H., Brindle, P.K., Schnabel, C.A., Pritchard, C.E., Cleary, M.L., and van Deursen,
615   J.M. (1999). CREB binding protein interacts with nucleoporin-specific FG repeats that
616   activate transcription and mediate NUP98-HOXA9 oncogenicity. Mol Cell Biol *19*, 764-776.
617   Kawakami, K., and Noda, T. (2004). Transposition of the Tol2 element, an Ac-like element
618   from the Japanese medaka fish Oryzias latipes, in mouse embryonic stem cells. Genetics
619   *166*, 895-899.
620   Kroon, E., Thorsteinsdottir, U., Mayotte, N., Nakamura, T., and Sauvageau, G. (2001). NUP98-
621   HOXA9 expression in hemopoietic stem cells induces chronic and acute myeloid leukemias
622   in mice. The EMBO journal *20*, 350-361.
623   Krumlauf, R. (1994). Hox genes in vertebrate development. Cell *78*, 191-201.
624   Labokha, A.A., Gradmann, S., Frey, S., Hulsmann, B.B., Urlaub, H., Baldus, M., and Gorlich,
625   D. (2013). Systematic analysis of barrier-forming FG hydrogels from Xenopus nuclear pore
626   complexes. The EMBO journal *32*, 204-218.
627   Lam, D.H., and Aplan, P.D. (2001). NUP98 gene fusions in hematologic malignancies.
628   Leukemia *15*, 1689-1695.
629   Lapalombella, R., Sun, Q., Williams, K., Tangeman, L., Jha, S., Zhong, Y., Goettl, V.,
630   Mahoney, E., Berglund, C., Gupta, S., *et al.* (2012). Selective inhibitors of nuclear export
631   show that CRM1/XPO1 is a target in chronic lymphocytic leukemia. Blood *120*, 4621-4634.
632   Lavau, C.P., Aumann, W.K., Sze, S.K., Gupta, V., Ripple, K., Port, S.A., Kehlenbach, R.H.,
633   and Wechsler, D.S. (2020). The SQSTM1-NUP214 fusion protein interacts with Crm1,
634   activates Hoxa and Meis1 genes, and drives leukemogenesis in mice. PloS one *15*,
635   e0232036.
636   Matkar, S., Thiel, A., and Hua, X. (2013). Menin: a scaffold protein that controls gene
637   expression and cell signaling. Trends Biochem Sci *38*, 394-402.
638   Mendes, A., and Fahrenkrog, B. (2019). NUP214 in Leukemia: It's More than Transport. Cells
639   *8*.
640   Mendes, A., Juhlen, R., Bousbata, S., and Fahrenkrog, B. (2020). Disclosing the Interactome of
641   Leukemogenic NUP98-HOXA9 and SET-NUP214 Fusion Proteins Using a Proteomic
642   Approach. Cells *9*.
643   Mendonca, J., Sharma, A., Kim, H.S., Hammers, H., Meeker, A., De Marzo, A., Carducci, M.,
644   Kauffman, M., Shacham, S., and Kachhap, S. (2014). Selective inhibitors of nuclear export
645   (SINE) as novel therapeutics for prostate cancer. Oncotarget *5*, 6102-6112.
646   Meszaros, B., Erdos, G., and Dosztanyi, Z. (2018). IUPred2A: context-dependent prediction of
647   protein disorder as a function of redox state and protein binding. Nucleic acids research *46*,
648   W329-W337.

649 Michmerhuizen, N.L., Klco, J.M., and Mullighan, C.G. (2020). Mechanistic insights and
650   potential therapeutic approaches for NUP98-rearranged hematologic malignancies. Blood
651   *136*, 2275-2289.
652 Mohammed, H., D'Santos, C., Serandour, A.A., Ali, H.R., Brown, G.D., Atkins, A., Rueda,
653   O.M., Holmes, K.A., Theodorou, V., Robinson, J.L.*, et al.* (2013). Endogenous purification
654   reveals GREB1 as a key estrogen receptor regulatory factor. Cell reports *3*, 342-349.
655 Mohammed, H., Taylor, C., Brown, G.D., Papachristou, E.K., Carroll, J.S., and D'Santos, C.S.
656   (2016). Rapid immunoprecipitation mass spectrometry of endogenous proteins (RIME) for
657   analysis of chromatin complexes. Nat Protoc *11*, 316-326.
658 Nakamura, T., Largaespada, D.A., Lee, M.P., Johnson, L.A., Ohyashiki, K., Toyama, K., Chen,
659   S.J., Willman, C.L., Chen, I.M., Feinberg, A.P.*, et al.* (1996). Fusion of the nucleoporin gene
660   NUP98 to HOXA9 by the chromosome translocation t(7;11)(p15;p15) in human myeloid
661   leukaemia. Nature genetics *12*, 154-158.
662 Niwa, H., Masui, S., Chambers, I., Smith, A.G., and Miyazaki, J. (2002). Phenotypic
663   complementation establishes requirements for specific POU domain and generic
664   transactivation function of Oct-3/4 in embryonic stem cells. Mol Cell Biol *22*, 1526-1536.
665 Ogawa, K., Matsui, H., Ohtsuka, S., and Niwa, H. (2004). A novel mechanism for regulating
666   clonal propagation of mouse ES cells. Genes to cells : devoted to molecular & cellular
667   mechanisms *9*, 471-477.
668 Oka, M., Asally, M., Yasuda, Y., Ogawa, Y., Tachibana, T., and Yoneda, Y. (2010). The mobile
669   FG nucleoporin Nup98 is a cofactor for Crm1-dependent protein export. Molecular biology
670   of the cell *21*, 1885-1896.
671 Oka, M., Mura, S., Otani, M., Miyamoto, Y., Nogami, J., Maehara, K., Harada, A., Tachibana,
672   T., Yoneda, Y., and Ohkawa, Y. (2019). Chromatin-bound CRM1 recruits SET-Nup214 and
673   NPM1c onto HOX clusters causing aberrant HOX expression in leukemia cells. eLife *8*.
674 Oka, M., Mura, S., Yamada, K., Sangel, P., Hirata, S., Maehara, K., Kawakami, K., Tachibana,
675   T., Ohkawa, Y., Kimura, H.*, et al.* (2016). Chromatin-prebound Crm1 recruits Nup98-
676   HoxA9 fusion to induce aberrant expression of Hox cluster genes. eLife *5*, e09540.
677 Ossareh-Nazari, B., Bachelerie, F., and Dargemont, C. (1997). Evidence for a role of CRM1 in
678   signal-mediated nuclear protein export. Science *278*, 141-144.
679 Pascual-Garcia, P., Jeong, J., and Capelson, M. (2014). Nucleoporin Nup98 Associates with
680   Trx/MLL and NSL Histone-Modifying Complexes and Regulates Hox Gene Expression.
681   Cell reports.
682 Port, S.A., Mendes, A., Valkova, C., Spillner, C., Fahrenkrog, B., Kaether, C., and Kehlenbach,
683   R.H. (2016). The Oncogenic Fusion Proteins SET-Nup214 and Sequestosome-1 (SQSTM1)-
684   Nup214 Form Dynamic Nuclear Bodies and Differentially Affect Nuclear Protein and
685   Poly(A)+ RNA Export. The Journal of biological chemistry *291*, 23068-23083.
686 Rio-Machin, A., Gomez-Lopez, G., Munoz, J., Garcia-Martinez, F., Maiques-Diaz, A., Alvarez,
687   S., Salgado, R.N., Shrestha, M., Torres-Ruiz, R., Haferlach, C.*, et al.* (2017). The molecular
688   pathogenesis of the NUP98-HOXA9 fusion protein in acute myeloid leukemia. Leukemia *31*,
689   2000-2005.

690   Sabari, B.R., Dall'Agnese, A., Boija, A., Klein, I.A., Coffey, E.L., Shrinivas, K., Abraham, B.J.,
691   Hannett, N.M., Zamudio, A.V., Manteiga, J.C.*, et al.* (2018). Coactivator condensation at
692   super-enhancers links phase separation and gene control. Science *361*.
693   Saito, S., Cigdem, S., Okuwaki, M., and Nagata, K. (2016). Leukemia-Associated Nup214
694   Fusion Proteins Disturb the XPO1-Mediated Nuclear-Cytoplasmic Transport Pathway and
695   Thereby the NF-kappaB Signaling Pathway. Mol Cell Biol *36*, 1820-1835.
696   Saito, S., Miyaji-Yamaguchi, M., and Nagata, K. (2004). Aberrant intracellular localization of
697   SET-CAN fusion protein, associated with a leukemia, disorganizes nuclear export.
698   International journal of cancer Journal international du cancer *111*, 501-507.
699   Schlenk, R.F., Dohner, K., Krauter, J., Frohling, S., Corbacioglu, A., Bullinger, L., Habdank,
700   M., Spath, D., Morgan, M., Benner, A.*, et al.* (2008). Mutations and treatment outcome in
701   cytogenetically normal acute myeloid leukemia. N Engl J Med *358*, 1909-1918.
702   Schmidt, H.B., and Gorlich, D. (2015). Nup98 FG domains from diverse species spontaneously
703   phase-separate into particles with nuclear pore-like permselectivity. eLife *4*.
704   Shanmugam, K., Green, N.C., Rambaldi, I., Saragovi, H.U., and Featherstone, M.S. (1999).
705   PBX and MEIS as non-DNA-binding partners in trimeric complexes with HOX proteins.
706   Mol Cell Biol *19*, 7577-7588.
707   Shima, Y., Yumoto, M., Katsumoto, T., and Kitabayashi, I. (2017). MLL is essential for
708   NUP98-HOXA9-induced leukemia. Leukemia *31*, 2200-2210.
709   Stade, K., Ford, C.S., Guthrie, C., and Weis, K. (1997). Exportin 1 (Crm1p) is an essential
710   nuclear export factor. Cell *90*, 1041-1050.
711   Tai, Y.T., Landesman, Y., Acharya, C., Calle, Y., Zhong, M.Y., Cea, M., Tannenbaum, D.,
712   Cagnetta, A., Reagan, M., Munshi, A.A.*, et al.* (2014). CRM1 inhibition induces tumor cell
713   cytotoxicity and impairs osteoclastogenesis in multiple myeloma: molecular mechanisms and
714   therapeutic implications. Leukemia *28*, 155-165.
715   Takeda, A., Goolsby, C., and Yaseen, N.R. (2006). NUP98-HOXA9 induces long-term
716   proliferation and blocks differentiation of primary human CD34+ hematopoietic cells.
717   Cancer research *66*, 6628-6637.
718   Takeda, A., Sarma, N.J., Abdul-Nabi, A.M., and Yaseen, N.R. (2010). Inhibition of CRM1-
719   mediated nuclear export of transcription factors by leukemogenic NUP98 fusion proteins.
720   The Journal of biological chemistry *285*, 16248-16257.
721   Terlecki-Zaniewicz, S., Humer, T., Eder, T., Schmoellerl, J., Heyes, E., Manhart, G., Kuchynka,
722   N., Parapatics, K., Liberante, F.G., Muller, A.C.*, et al.* (2021). Biomolecular condensation of
723   NUP98 fusion proteins drives leukemogenic gene expression. Nat Struct Mol Biol *28*, 190-
724   201.
725   Turner, J.G., Dawson, J., Emmons, M.F., Cubitt, C.L., Kauffman, M., Shacham, S., Hazlehurst,
726   L.A., and Sullivan, D.M. (2013). CRM1 Inhibition Sensitizes Drug Resistant Human
727   Myeloma Cells to Topoisomerase II and Proteasome Inhibitors both In Vitro and Ex Vivo.
728   Journal of Cancer *4*, 614-625.

729 Urasaki, A., Morvan, G., and Kawakami, K. (2006). Functional dissection of the Tol2
730   transposable element identified the minimal cis-sequence and a highly repetitive sequence in
731   the subterminal region essential for transposition. Genetics *174*, 639-649.
732 Van Vlierberghe, P., van Grotel, M., Tchinda, J., Lee, C., Beverloo, H.B., van der Spek, P.J.,
733   Stubbs, A., Cools, J., Nagata, K., Fornerod, M.*, et al.* (2008). The recurrent SET-NUP214
734   fusion as a new HOXA activation mechanism in pediatric T-cell acute lymphoblastic
735   leukemia. Blood *111*, 4668-4680.
736 von Lindern, M., van Baal, S., Wiegant, J., Raap, A., Hagemeijer, A., and Grosveld, G. (1992).
737   Can, a putative oncogene associated with myeloid leukemogenesis, may be activated by
738   fusion of its 3' half to different genes: characterization of the set gene. Mol Cell Biol *12*,
739   3346-3355.
740 Xu, H., Valerio, D.G., Eisold, M.E., Sinha, A., Koche, R.P., Hu, W., Chen, C.W., Chu, S.H.,
741   Brien, G.L., Park, C.Y.*, et al.* (2016). NUP98 Fusion Proteins Interact with the NSL and
742   MLL1 Complexes to Drive Leukemogenesis. Cancer cell *30*, 863-878.
743 Xu, S., and Powers, M.A. (2009). Nuclear pore proteins and cancer. Semin Cell Dev Biol *20*,
744   620-630.
745 Yano, T., Nakamura, T., Blechman, J., Sorio, C., Dang, C.V., Geiger, B., and Canaani, E.
746   (1997). Nuclear punctate distribution of ALL-1 is conferred by distinct elements at the N
747   terminus of the protein. Proceedings of the National Academy of Sciences of the United
748   States of America *94*, 7286-7291.
749 Yokoyama, A., Kitabayashi, I., Ayton, P.M., Cleary, M.L., and Ohki, M. (2002). Leukemia
750   proto-oncoprotein MLL is proteolytically processed into 2 fragments with opposite
751   transcriptional properties. Blood *100*, 3710-3718.
752 Yokoyama, A., Somervaille, T.C., Smith, K.S., Rozenblatt-Rosen, O., Meyerson, M., and
753   Cleary, M.L. (2005). The menin tumor suppressor protein is an essential oncogenic cofactor
754   for MLL-associated leukemogenesis. Cell *123*, 207-218.
755 Zhang, K., Wang, M., Tamayo, A.T., Shacham, S., Kauffman, M., Lee, J., Zhang, L., Ou, Z., Li,
756   C., Sun, L.*, et al.* (2013). Novel selective inhibitors of nuclear export CRM1 antagonists for
757   therapy in mantle cell lymphoma. Exp Hematol *41*, 67-78 e64.
758 Zhou, M.H., and Yang, Q.M. (2014). NUP214 fusion genes in acute leukemia (Review). Oncol
759   Lett *8*, 959-962.

760
761
762 **FIGURE LEGENDS**
763
764 **Figure 1. SET-NUP214 and CRM1 physically and functionally associate with MLL1.**
765 (A, B) Subcellular localization of SET-NUP214 and *HOX-B* or *RNF2* (control) gene loci in
766 LOUCY cells.
767 (A) ImmunoFISH was performed to detect SET-NUP214 nuclear bodies and respective gene
768 loci. *HOX-B* cluster region is frequently found adjacent to SET-NUP214 nuclear bodies as
769 compared with *RNF2*. Nuclei were stained with DAPI. Scale bars: 10 µm. (B) The minimum

19

770   distance between each gene locus (as revealed by FISH) and the closest SET-NUP214 nuclear

771   bodies was analyzed using ImageJ. (C) Schematic of RIME used in this study. (D) Summary of

772   the RIME results. (E) Effect of knockdown of candidate components of SET-NUP214 nuclear

773   bodies. Knockdown of ADAR1, KMT2A, STRN, MX2, and TARFIP3 was performed by

774   nucleofection of siRNA (IDT) in LOUCY cells. The effect of knockdown on *HOX* gene

775   expression (*HOXA9*, *HOXA11*, *HOXB4*, and *HOXB9*) was examined 4 days after nucleofection.

776   *GAPDH* was used as the reference gene. The data are the average of two biological replicates

777   each with two technical replicates.

778

779   **Figure 1—figure supplement 1**

780   Validation of knockdown by western blot analysis.

781   Knockdown of indicated proteins were examined 4 days after nucleofection with either

782   negative control siRNA or siRNA (DsiRNA, IDT) against targets by immunoblotting using

783   indicated antibodies.

784

785   **Figure 2. SET-NUP214 nuclear bodies colocalized with CRM1, MLL1 and Menin.**

786   LOUCY cells were immunostained with anti-NUP214, MLL1C, Menin, BRD4, and CRM1

787   antibodies. The merged images of CRM1 are shown. Nuclei were stained with DAPI. Scale bar:

788   5 μm.

789

790   **Figure 3. MLL1 is an essential component of SET-NUP214 nuclear bodies to recruit and**

791   **activate target genes.**

792   (A) The binding profiles of NUP214, CRM1, and MLL1C in LOUCY cells treated either in the

793   presence of DMSO (vehicle control) or KPT-330 (1,000 nM) for 24 h (ChIP-seq data for

794   NUP214 and CRM1 were from previous study: GSE127983.) (B) Aggregation plots of CRM1

795   and MLL1C binding sites in LOUCY. CRM1 binding signals and MLL1C binding signals are

796   mapped against NUP214 binding sites. (C) ChIP-qPCR analysis of CRM1, NUP214, and MLL1

797   at *HOX* gene loci in LOUCY cells treated either with control siRNA or MLL1 siRNA for 4

798   days. The primer set used was as follows: HOXA4A5 (intergenic region between *HOXA4* and

799   *HOXA5*); HOXA9 (promoter); HOXB4 (promoter); HOXB4 (enhancer); HOXB9 (promoter).

800   Data are presented as mean values ± SEM of three independent experiments (n = 3).

801

802   **Figure 4. The effect of CRM1 inhibitor on the function of SET-NUP214 nuclear bodies.**

803   (A) LOUCY cells treated with DMSO, 100 or 1,000 nM of KPT-330 for 24 h were co-

804   immunostained with anti-CRM1 and MLL1C antibodies. DAPI staining was used to visualize

805   nuclei. Scale bar: 5 μm.

806   (B) ChIP-qPCR analysis of CRM1, NUP214, and MLL1C at *HOX* gene loci in LOUCY cells

807   cultured either in the presence of DMSO (vehicle control) or KPT-330 (1,000 nM) for 24 h.

808   Data are presented as mean values ± SEM of three independent experiments (n = 3). (C)

809   Protein expression levels of MLL1N, MLL1C, CRM1, SET-NUP214, and GAPDH in LOUCY

810   cells treated with DMSO (vehicle control for KPT-330) or KPT-330 (100 or 1,000 nM), EtOH

811 (vehicle control for LMB) or LMB (10 nM) for 24 h. The cell lysates were prepared in RIPA

812 buffer and analyzed by immunoblotting.

813

814 **Figure 5. FG repeat and homeodomain of NUP98-HOXA9 is important for its**

815 **accumulation on HOX clusters and gene activation.**

816 (A) qPCR analysis of NUP98-HOXA9-target genes (*Hoxa9*, *Hoxa10*, *Hoxb4*, *Hoxb8*, *Meis1*,

817 *Pbx3*) in indicated NUP98-HOXA9 expressing stable cell lines. Two independent cell lines for

818 each (control, wild-type NUP98-HOXA9, AG mutant, and N51S homeodomain mutant) were

819 analyzed. *Gapdh* was used as a reference gene. (B) Schematic representation of NUP98-

820 HOXA9, FG mutant, or homeodomain (N51S) mutant. (C) (left) Confocal imaging of FLAG-

821 NUP98-HOXA9, AG mutant, or N51S mutant. DAPI staining was used to visualize the nuclei.

822 (right) Protein expression levels of FLAG-NUP98-HOXA9 and its mutants. GAPDH was used

823 as a loading control. (D) Binding profiles of FLAG-NUP98-HOXA9, AG mutant, or N51S

824 mutant in mESC stable cell lines.

825

826 **Figure 6. NUP98-HOXA9 nuclear bodies stimulate the condensation of MLL1 and its**

827 **accumulation on target sites.**

828 (A) Subcellular localization of MLL1C in stable mESCs. Parental mESCs or its stable cell lines

829 expressing FLAG-NUP98-HOXA9, AG mutant, homeodomain mutant, were co-immunostained

830 with anti-MLL1C and FLAG. DAPI staining for nuclei. (B–D) The binding profiles of MLL1C,

831 MLL1N, CRM1 in parental mESC or stable cell lines expressing FLAG-NUP98-HOXA9 as

832 revealed with ChIP-seq (B:*Hoxa*, C:*Pbx3*, D:*Meis1*).

833

834 **Figure 6—figure supplement 1**

835 NUP98-HOXA9 nuclear bodies stimulate the condensation of MLL1 on *Hoxb* cluster.

836 The binding profiles of MLL1C, MLL1N, CRM1 on *Hoxb* cluster in parental mESC or stable

837 cell lines expressing FLAG-NUP98-HOXA9 as revealed with ChIP-seq.

838

839 **Figure 7. The formation of NUP98-HOXA9 nuclear bodies with an intact homeodomain is**

840 **important to enhance the recruitment of CRM1 and MLL1 on *Hox* region.**

841 (A) ChIP-qPCR analysis of CRM1, MLL1N and MLL1C at Hox cluster (*Hoxa2-a3*, *Hoxa4*,

842 *Hoxa9*) and intergenic control region (chr18) in mESCs stably expressing FLAG-NUP98-

843 HOXA9, AG mutant, homeodomain mutant (N51S). Two independent cell lines were used.

844 Data are presented as mean values ± SEM of three independent experiments (n = 3). Asterisks

845 indicate statistical significance determined by Student's t-test; * $p < 0.05$; ** $p < 0.01$; *** $p <$

846 0.001. (B) Correlation plots of MLL1N, MLL1C, and CRM1(CST) binding sites in parental

847 mESCs (Parental-ES) or NUP98-HOXA9-expressing mESCs (NHA9-ES), together with

848 FLAG-NUP98HOXA9, AG mutant, homeodomain mutant (N51S). (C) NUP98-HOXA9 or

849 SET-NUP214 forms molecular condensates with CRM1 and MLL1 on its target sites including

850 *Hox* cluster regions. In phase-separation-deficient mutant, neither the accumulation of NUP-

851 fusion, CRM1, MLL1 are observed. In DNA-binding deficient mutant, NUP-fusion can form

852   nuclear bodies, but those are not substantially associating with the chromatin of target genes.

853   Note that MLL1 is not recruited in these nuclear bodies.

854

855   **Figure 7—figure supplement 1**

856   The intrinsically disordered regions of MLL1s are predicted using IUPred3A (intrinsically

857   unstructured/disordered proteins and domains prediction tool). The cleavage sites of MLL1 are

858   shown by arrows.

859

860   **Table I.**

861   SET-NUP214 or CRM1 associated proteins in LOUCY cells were identified using RIME. For

862   each target protein, RIME was performed in duplicate using specific antibodies or control IgG,

863   and the number of peptides identified and sequence coverage are shown. Nucleoporins and

864   nuclear transport–related proteins are indicated by blue letters. Several proteins (red letters) are

865   not involved in the nuclear transport activity.

866
867

Figure 1. SET-NUP214 and CRM1 physically and functionally associate with MLL1.
(A, B) Subcellular localization of SET-NUP214 and HOX-B or RNF2 (control) gene loci in LOUCY cells.
(A) ImmunoFISH was performed to detect SET-NUP214 nuclear bodies and respective gene loci. HOX-B cluster region is frequently found adjacent to SET-NUP214 nuclear bodies as compared with RNF2. Nuclei were stained with DAPI. Scale bars: 10 μm. (B) The minimum distance between each gene locus (as revealed by FISH) and the closest SET-NUP214 nuclear bodies was analyzed using ImageJ. (C) Schematic of RIME used in this study. (D) Schematic summary of the RIME results. (E) Effect of knockdown of candidate components of SET-NUP214 nuclear bodies. Knockdown of ADAR1, KMT2A, STRN, MX2, and TARFIP3 was performed by nucleofection of siRNA (IDT) in LOUCY cells. The effect of knockdown on HOX gene expression (HOXA9, HOXA11, HOXB4, and HOXB9) was examined 4 days after nucleofection. GAPDH was used as the reference gene. The data are the average of two biological replicates each with two technical replicates.
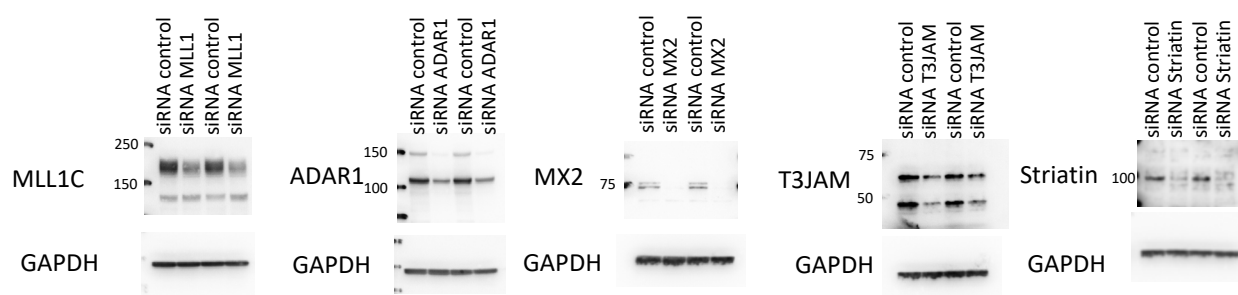
Figure 1—figure supplement 1
Validation of knockdown by western blot analysis.
Knockdown of indicated proteins were examined 4 days after nucleofection with either negative control siRNA or siRNA (DsiRNA, IDT) against targets by immunoblotting using indicated antibodies.
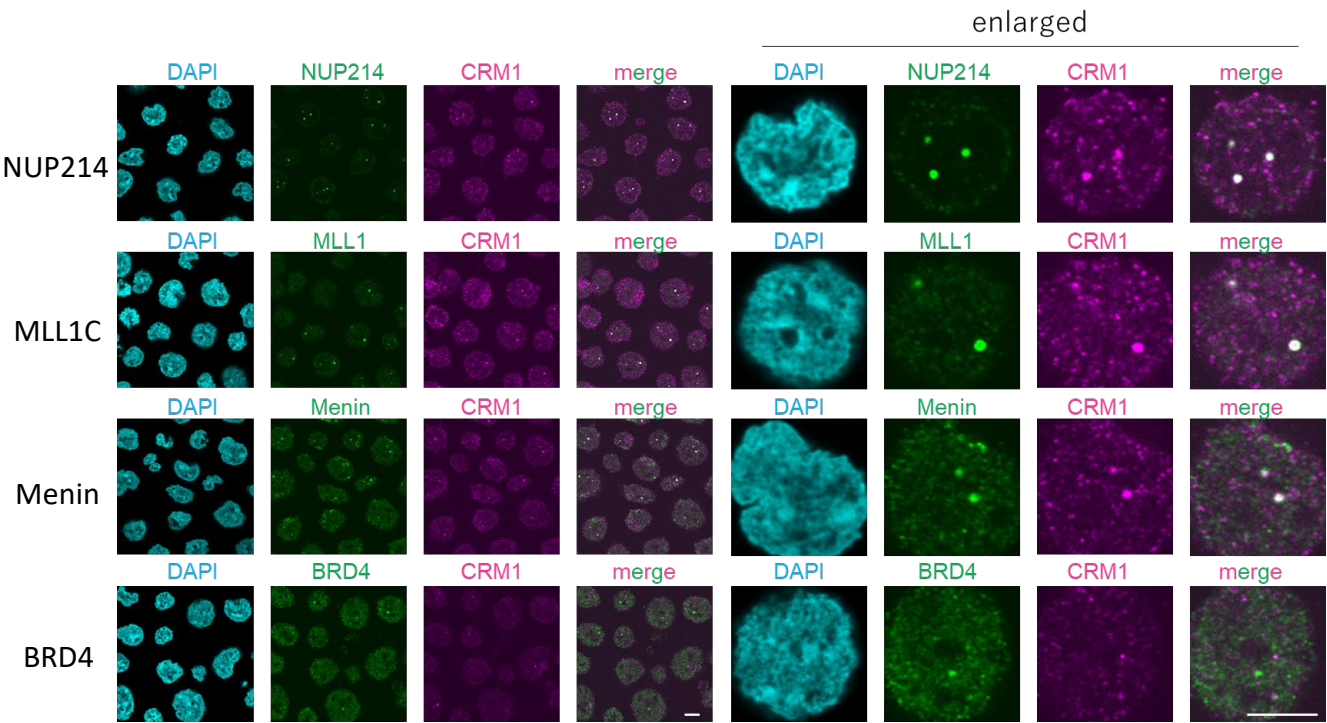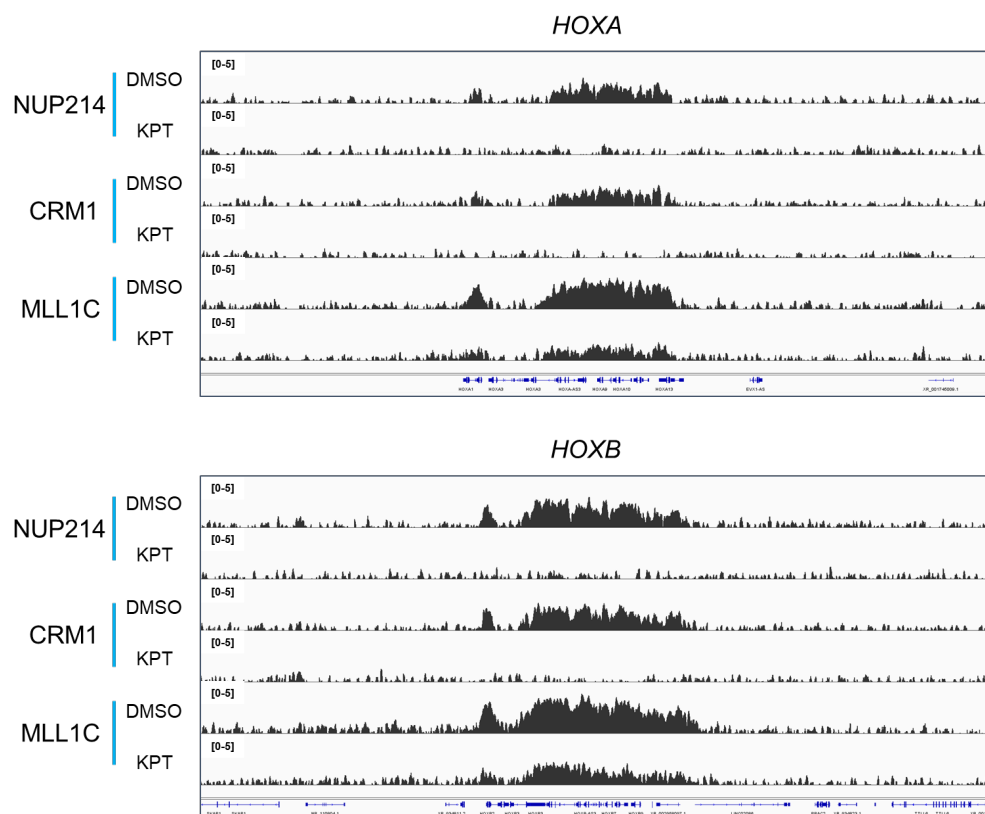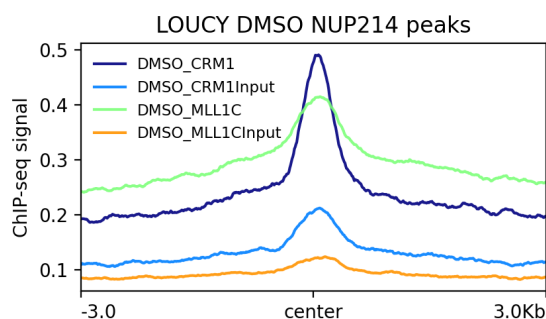
Figure 2. SET-NUP214 nuclear bodies colocalized with CRM1, MLL1 and Menin.
LOUCY cells were immunostained with anti-NUP214, MLL1C, Menin, BRD4, and CRM1 antibodies.
The merged images of CRM1 are shown. Nuclei were stained with DAPI. Scale bar: 5 μm.
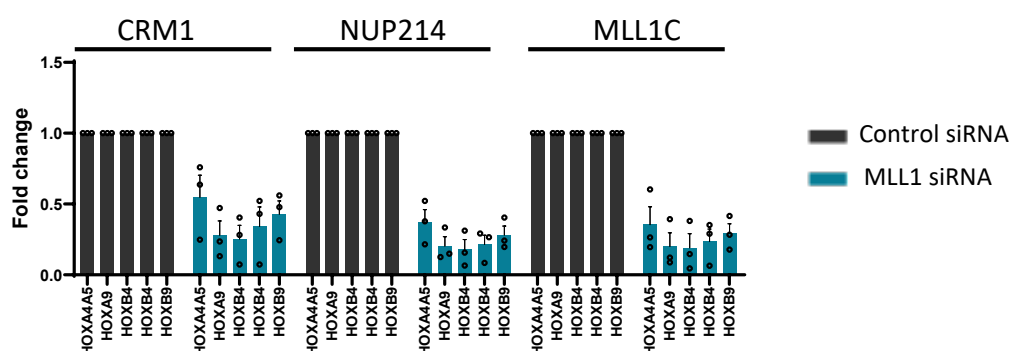
Figure 3. MLL1 is an essential component of SET-NUP214 nuclear bodies to recruit and activate target genes.
(A) The binding profiles of NUP214, CRM1, and MLL1C in LOUCY cells treated either in the presence of DMSO (vehicle control) or KPT-330 (1,000 nM) for 24 h (ChIP-seq data for NUP214 and CRM1 were from previous study: GSE127983.) (B) Aggregation plots of CRM1 and MLL1C binding sites in LOUCY. CRM1 binding signals and MLL1C binding signals are mapped against Nup214 binding sites. (C) ChIP-qPCR analysis of CRM1, NUP214, and MLL1 at HOX gene loci in LOUCY cells treated either with control siRNA or MLL1 siRNA for 4 days. The primer set used was as follows: HOXA4A5 (intergenic region between HOXA4 and HOXA5); HOXA9 (promoter); HOXB4 (promoter); HOXB4 (enhancer); HOXB9 (promoter). Data are presented as mean values ± SEM of three independent experiments (n = 3).
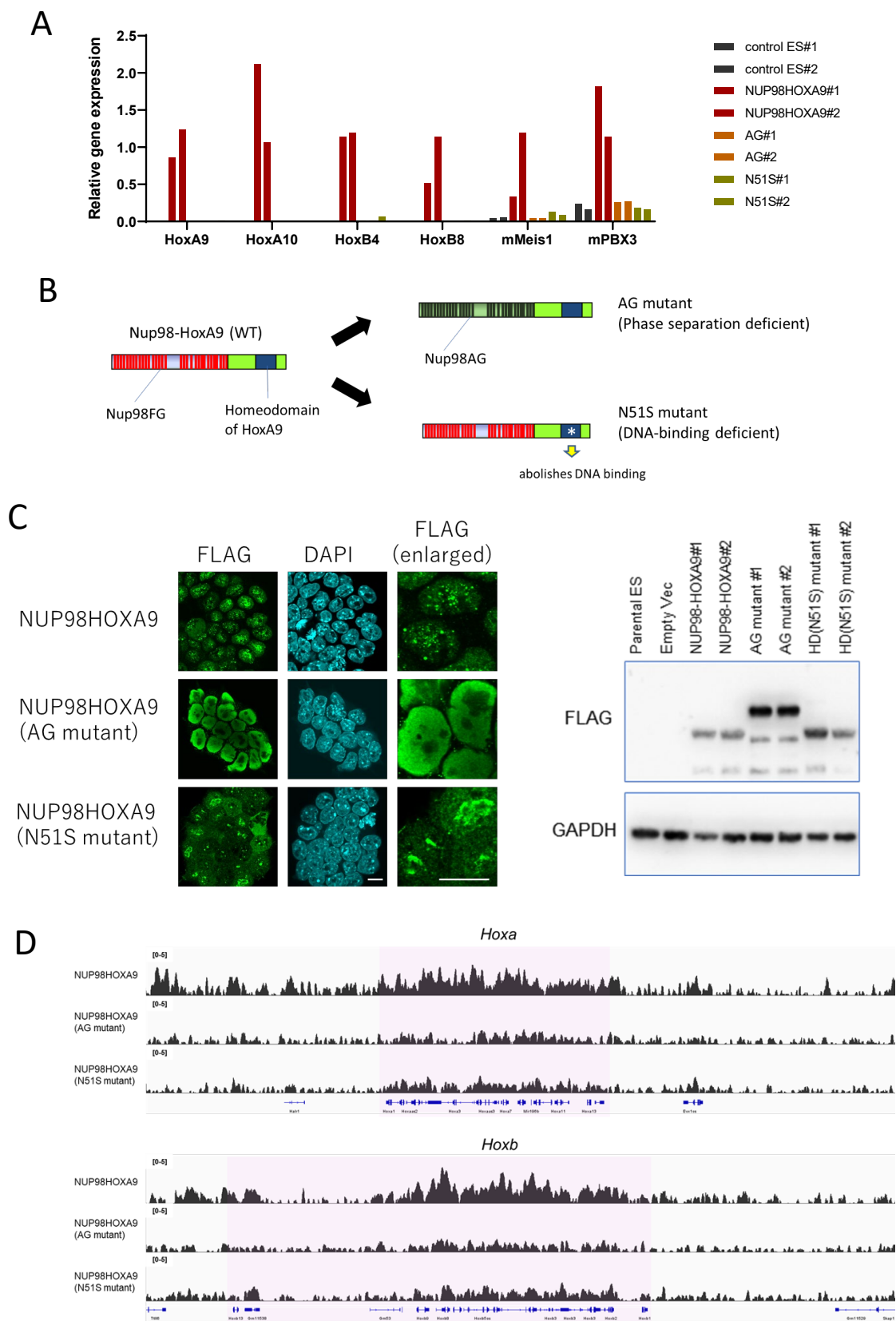
Figure 4. The effect of CRM1 inhibitor on the function of SET-NUP214 nuclear bodies.
(A) LOUCY cells treated with DMSO, 100 or 1,000 nM of KPT-330 for 24 h were co-immunostained with anti-CRM1 and MLL1C antibodies. DAPI staining was used to visualize nuclei. Scale bar: 5 μm. (B) ChIP-qPCR analysis of CRM1, NUP214, and MLL1C at HOX gene loci in LOUCY cells cultured either in the presence of DMSO (vehicle control) or KPT-330 (1,000 nM) for 24 h. Data are presented as mean values ± SEM of three independent experiments (n = 3). (C) Protein expression levels of MLL1N, MLL1C, CRM1, SET-NUP214, and GAPDH in LOUCY cells treated with DMSO (vehicle control for KPT-330) or KPT-330 (100 or 1,000 nM), EtOH (vehicle control for LMB) or LMB (10 nM) for 24 h. The cell lysates were prepared in RIPA buffer and analyzed by immunoblotting.

Figure 5. FG repeat and homeodomain of NUP98-HOXA9 is important for its accumulation on *HOX* clusters and gene activation.

(A) qPCR analysis of NUP98-HOXA9-target genes (HOXA9, HOXA10, HOXB4, HOXB8, Meis1, Pbx3) in indicated NUP98-HOXA9 expressing stable cell lines. Two independent cell lines for each (control, wild-type NUP98-HOXA9, AG mutant, and N51S homeodomain mutant) were analyzed. GAPDH was used as a reference gene. (B) Schematic representation of NUP98-HOXA9, FG mutant, or homeodomain (N51S) mutant. (C) (left) Confocal imaging of FLAG-NUP98-HOXA9, AG mutant, or N51S mutant. DAPI staining was used to visualize the nuclei. (right) Protein expression levels of FLAG-NUP98-HOXA9 and its mutants. GAPDH was used as a loading control. (D) Binding profiles of FLAG-NUP98-HOXA9, AG mutant, or N51S mutant in mESC stable cell lines.
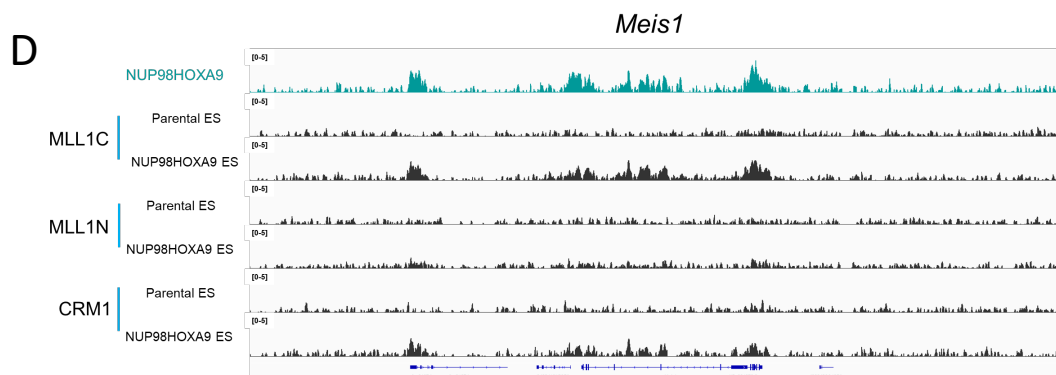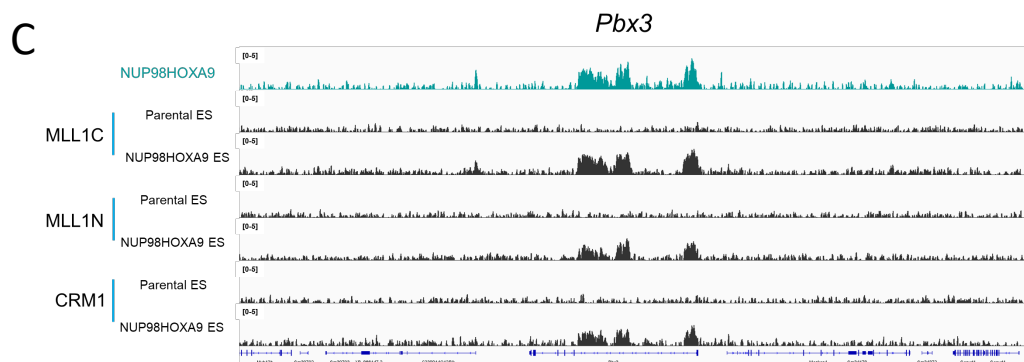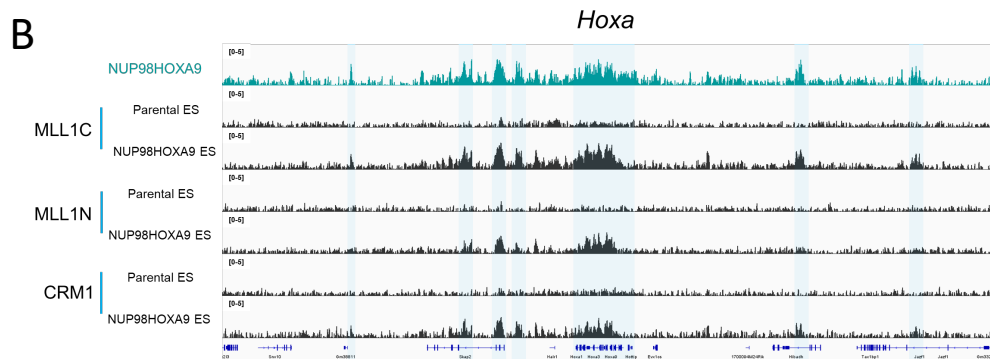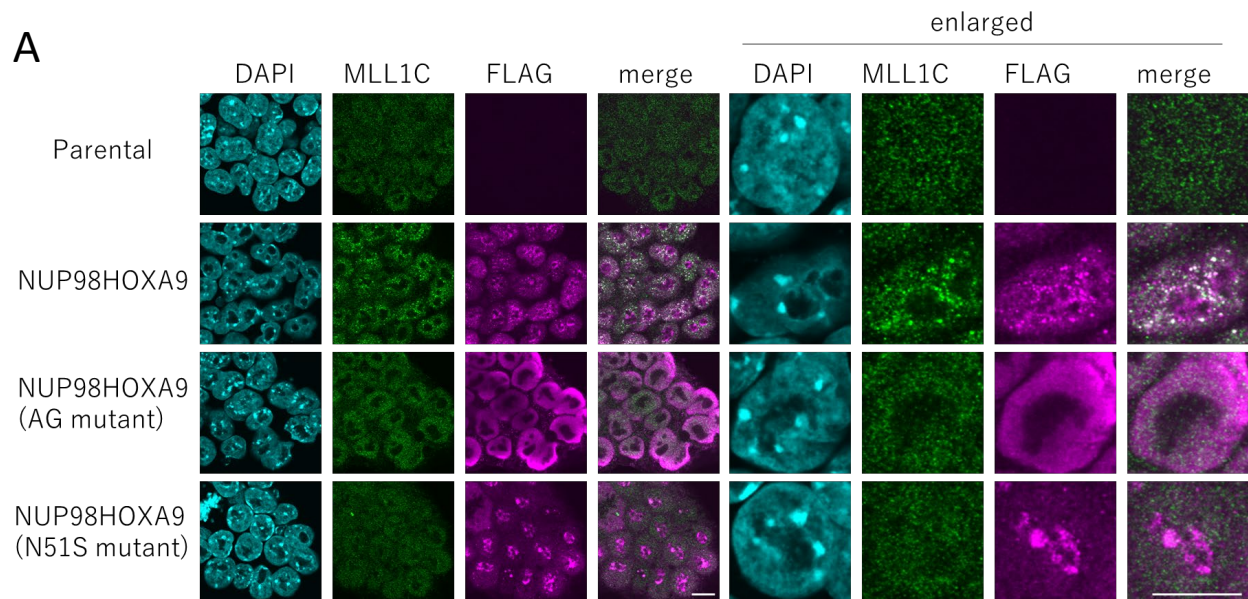
Figure 6. NUP98-HOXA9 nuclear bodies stimulate the condensation of MLL1 and its accumulation on target sites.
(A) Subcellular localization of MLL1C in stable mESCs. Parental mESCs or its stable cell lines expressing FLAG-NUP98-HOXA9, AG mutant, homeodomain mutant, were co-immunostained with anti-MLL1C and FLAG. DAPI staining for nuclei. (B–D) The binding profiles of MLL1C, MLL1N, CRM1 in parental mESC or stable cell lines expressing FLAG-NUP98-HOXA9 as revealed with ChIP-seq (B:*Hoxa*, C:*Pbx3*, D:*Meis1*).
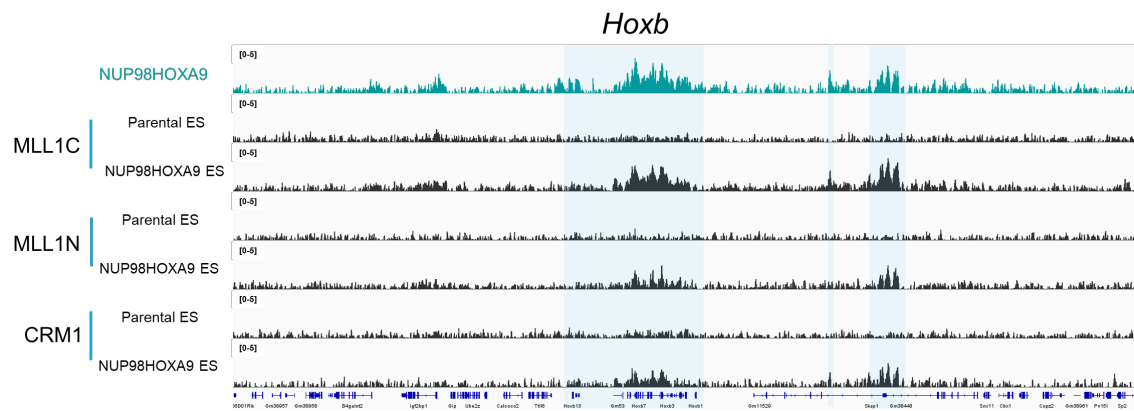
Figure 6—figure supplement 1
NUP98-HOXA9 nuclear bodies stimulate the condensation of MLL1 on *hoxb* cluster.
The binding profiles of MLL1C, MLL1N, CRM1 on Hoxb cluster in parental mESC or stable cell lines expressing FLAG-NUP98-HOXA9 as revealed with ChIP-seq.
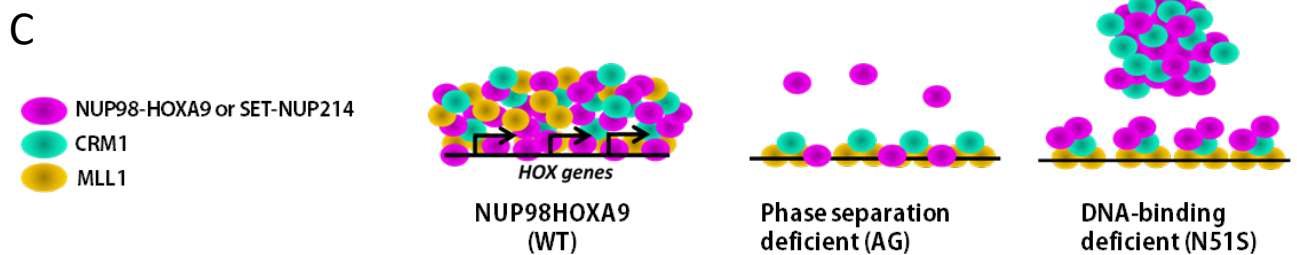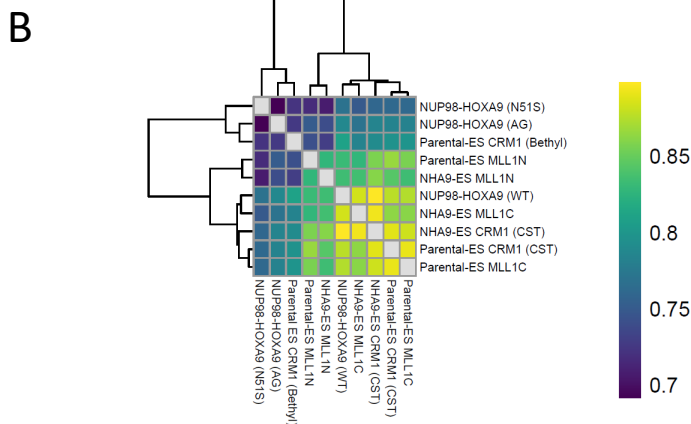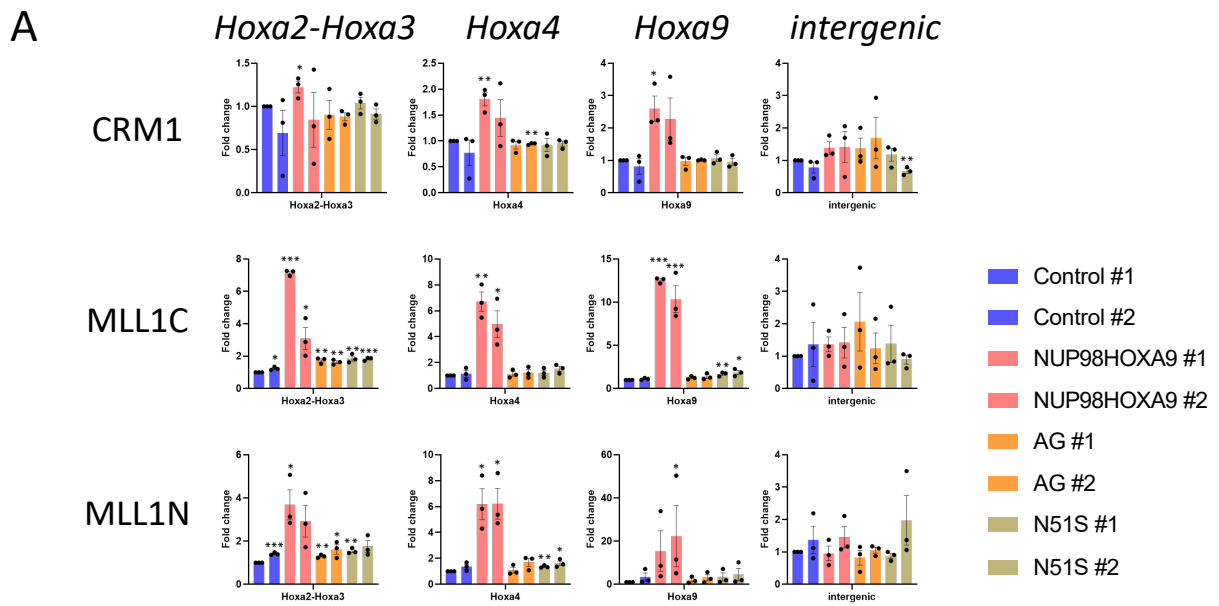
Figure 7. The formation of NUP98-HOXA9 nuclear bodies with an intact homeodomain is important to enhance the recruitment of CRM1 and MLL1 on *Hox* region.

(A) ChIP-qPCR analysis of CRM1, MLL1N and MLL1C at Hox cluster (Hoxa2-a3, Hoxa4, Hoxa9) and intergenic control region (chr18) in mESCs stably expressing FLAG-NUP98-HOXA9, AG mutant, homeodomain mutant. Two independent cell lines were used. Data are presented as mean values $\pm$ SEM of three independent experiments (n = 3). (B) Correlation plots of MLL1N, MLL1C, and CRM1(CST) binding sites in parental mESCs (Parental-ES) or NUP98-HOXA9-expressing mESCs (NHA9-ES), together with FLAG-NUP98HOXA9, AG mutant, homeodomain mutant (N51S). (C) NUP98-HOXA9 or SET-NUP214 forms molecular condensates with CRM1 and MLL1 on its target sites including HOX cluster regions. In phase-separation-deficient mutant, neither the accumulation of NUP-fusion, CRM1, MLL1 are observed. In DNA-binding deficient mutant, NUP-fusion can form nuclear bodies, but those are not substantially associating with the chromatin of target genes. Note that MLL1 is not recruited in these nuclear bodies.

Homo sapiens lysine methyltransferase 2A (KMT2A), transcript variant 1 (NM_001197104.2)
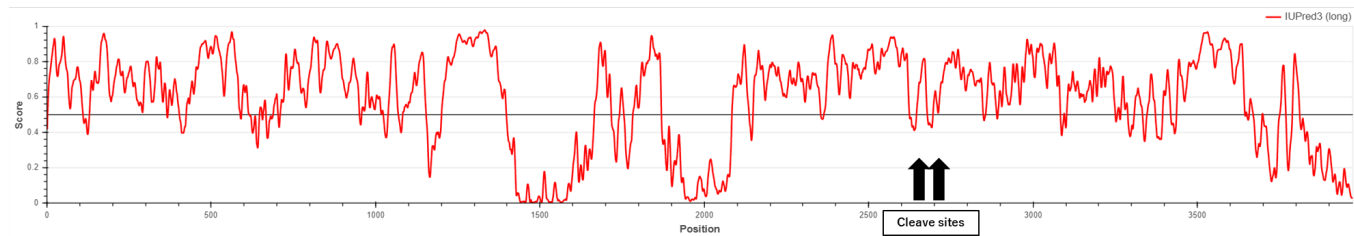
Mus musculus lysine (K)-specific methyltransferase 2A (Kmt2a), NM_001357549.2
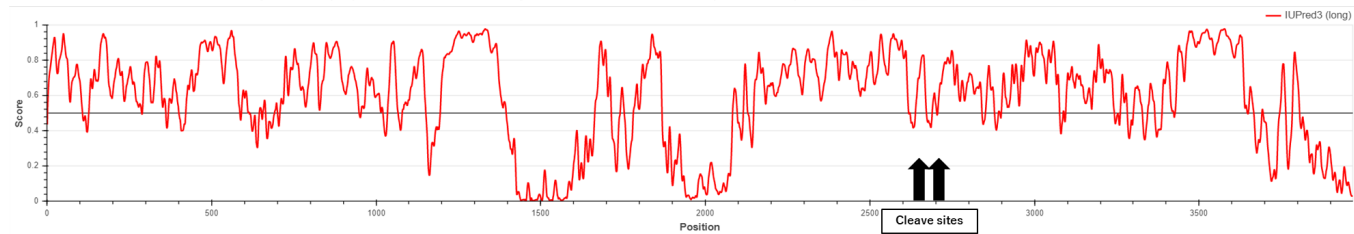

Figure 7—figure supplement 1
The intrinsically disordered regions of MLL1s are predicted using IUPred3A (intrinsically unstructured/disordered proteins and domains prediction tool).
The cleavage sites of MLL1 are shown by arrows.

Table I.
SET-NUP214 or CRM1 associated proteins in LOUCY cells were identified using RIME. For each target protein, RIME was performed in duplicate using specific antibodies or control IgG, and the number of peptides identified and sequence coverage are shown. Nucleoporins and nuclear transport–related proteins are indicated by blue letters. Several proteins (red letters) are not involved in the nuclear transport activity.

Gene names	Control(1)	Control(2)	NUP214(1)	NUP214(2)	CRM1(1)	CRM1(2)	Sequence coverage [%] (NUP214)	Sequence coverage [%](CRM1)	Mol. weight [kDa]
RANBP2	15	12	133	144	227	221	47.5	60.8	358.2
NUP214	13	9	81	86	79	81	50.2	43.5	212.57
TPR	4	6	48	71	118	67	33.9	50.2	267.29
XPO1	4	6	36	39	59	61	40.8	47.6	123.38
NUP98	3	4	35	41	42	35	28.7	29.4	195.82
NUP210	5	5	34	34	32	18	24.3	23	205.11
NUP93	2	3	32	37	32	28	46.6	39.8	93.487
ADAR	1	1	32	32	14	11	31.8	16.4	103.64
NUP205	0	1	30	39	22	16	22.9	13	227.92
NUP88	0	0	26	28	19	15	40.2	32.8	83.541
NUP155	0	0	22	24	17	13	26	18	155.2
GLE1	1	0	22	26	8	4	41.4	16	79.835
MLL1	0	0	22	33	68	74	11.9	22.2	427.73
RANGAP1	1	1	20	22	35	38	46.3	51.1	63.541
NUP107	1	0	20	24	24	21	30.2	28.8	106.37
NUP153	0	2	17	20	54	54	17.3	41.6	149.39
STRN	0	0	16	20	25	16	34.6	45.4	86.131
KPNB1	0	1	15	19	24	24	24	27.5	97.169
MX2	0	0	15	17	24	19	29.7	38.3	82.088
NUP133	2	0	15	18	23	12	21.8	25.1	128.98
NUP54	0	1	14	14	19	14	35.1	38.1	55.435
RAN	6	6	13	13	19	19	37	43.1	24.423
NXF1	0	0	13	14	24	25	24.4	35.5	70.182
SET	2	2	12	13			46.9		32.103
NUP188	0	0	12	14	4	2	11.7	3.3	196.04
NUP62	1	1	11	11	10	7	21.5	18	53.254
TNPO1	2	2	11	13	16	16	14.5	15.5	102.35
NUP50	2	0	11	13	25	25	39.3	54.5	46.862
RAE1	1	0	10	12	9	10	40.2	37.2	40.968
TRAF3IP3	0	1	10	14	32	30	26.1	51.7	63.626
NUP35	0	0	9	10	11	9	44.5	45.1	34.773
NUP85	0	0	7	8	7	7	15.7	14	75.019
CSE1L	0	0	7	8	15	11	10.6	18.8	103.88
RANBP3	0	0	6	7	15	17	19	31.7	53.41
NUPL1	0	0	6	8	11	10	14	20.2	50.21
NUP160	0	0	6	10	7	4	10.9	4.7	162.12
NUP37	0	0	5	5	3	0	20.6	11.3	36.707
IPO5	0	0	5	7	4	2	8.2	6.1	125.54
KPNA3	0	0	4	5	7	7	8.3	14.8	57.81
TNPO3	0	1	4	6	4	3	7.8	5.1	102.54